Evaluating the biogeochemistry of dissolved inorganic carbon in the Canadian Arctic Archipelago using stable and radiocarbon isotopes

Author: Liam Jasperse
Supervisor: Dr. Brett Walker

In partial fulfillment of the requirements for the M.Sc. degree in Earth Sciences

Faculty of Science

Department of Earth and Environmental Sciences

University of Ottawa

Table of Contents

Statement of Authorship Contributions

This thesis was written by MSc. student Liam Jasperse (L.J.) and contains a submitted manuscript coauthored by Dr. Brent Else (B.E.), Jennifer Walker (J.W.), and supervisor Dr. Brett Walker (B.D.W.). All coauthors declare no conflict of interest through their contributions. We also declare no ethics approval is required. B.D.W. conceived the hypothesis and objectives of this investigation. L.J. wrote the paper with input from B.D.W. Manuscript comments were provided by B.E and J.W. Funding and logistics for the 2021 research cruise (Cruise# 2104, Leg 4) was managed by co-principal investigator B.E. Training, analysis assistance and data reduction was made possible thanks to the generous efforts and expertise provided by J.W. and B.D.W. We would also like to thank B.D.W for securing ship time for his students, providing the necessary research facilities, and coordinating coauthors on the attached manuscript.

Thesis Abstract

Human activity is unequivocally contributing to climate change and global warming (IPCC 2023). The oceans act to moderate climate by removing CO_2 (a greenhouse gas) from the atmosphere via air-sea gas exchange and sequestration as dissolved inorganic carbon (DIC). DIC is the largest actively cycling pool of carbon on Earth (38,000 Gt) and approximately half of all anthropogenic carbon emissions have already been absorbed by the world's oceans (IPCC 2023). Despite this, the Arctic is still warming at rates up to four times faster than the global average (Rantanen et al., 2022). Research suggests the Canadian Arctic Archipelago (CAA) is an important region for the marine carbon cycle (e.g. Papakyriakou & Miller, 2011; Zeidan et al., 2022) but its response to climate change remains poorly constrained. The CAA connects the Pacific, Arctic, and Atlantic Oceans. Melting permafrost, sea ice, changing biogeochemistry and increased freshwater flux within have the potential to impact local and global processes, such as deepwater formation in the North Atlantic and global thermohaline circulation (e.g. Serreze et al., 2006). Stable carbon ($\delta^{13}C$) and radiocarbon ($\Delta^{14}C$) in marine DIC are powerful tools for determining carbon sources and ageing. These isotopes can be used as tracers for processes such as water mass advection, biogeochemical modification, and anthropogenic carbon penetration. In this thesis, we present n = 151 DIC samples from the CAA (Beaufort Sea to Lancaster Sound) combined with n = 110 samples from Baffin Bay sampled by Zeidan and coworkers (2022) to make broad, pan-arctic carbon cycling interpretations. We offer the most complete, pan-arctic DIC isotope dataset available.

CAA DIC concentrations, $\delta^{13}C$ and $\Delta^{14}C$ values ranged between 1.79 to 2.65 mmol L^{-1}, -0.68 to +1.86‰, and -90.7 to +49.5‰ respectively. A general trend from West to East of decreasing DIC concentrations, decreasing $\delta^{13}C$ values and increasing $\Delta^{14}C$ was observed in

advecting Pacific water masses throughout the CAA. These isotopic trends suggest heterotrophic remineralization of "bomb" carbon-containing particulate organic matter from riverine influx is translated to the marine DIC pool in the CAA. The shallow, fresh Kitikmeot region is especially dominated by riverine influx, leading to low DIC concentrations (0.10 to 2.20 mmol L^{-1}) and positive $\Delta^{14}C$ (+5.0 to +6.8‰) with positive $\delta^{13}C$ (+0.30 to +0.99‰) from additional physical mixing processes unique to the region. In contrast, highly negative surface DIC $\Delta^{14}C$ values of -44.7‰ and -51.9‰ near the Mackenzie River suggest thawed permafrost carbon from this great Arctic river's expansive watershed is incorporated into marine DIC in the Beaufort Sea. Further North, we examine Parry Channel, an important region between M'Clure Strait and Lancaster Sound through which all CAA waters must flow before entering Baffin Bay. We hypothesize that our observed enrichment of both $\delta^{13}C$ and $\Delta^{14}C$ across the channel is either indicative of two distinct biogeochemical provinces separated by the shallow (~125m) Barrow Strait, or that underlying Atlantic waters are mixed vertically into shallower Pacific waters by the local bathymetry (as interpreted by Lehmann et al., 2022). In the Beaufort Sea, we use nearby historical data to propose anthropogenic carbon concentrations have increased in Canadian Arctic water masses since 2009, reaching new depths as low as 1500m, but that rates of uptake are decreasing by as much as eight times less than in 2012. This suggests the ocean's natural sink for CO_2 is weakening significantly on decadal timescales. Lastly, the stark contrast in DIC $\delta^{13}C$ and $\Delta^{14}C$ values between the Beaufort Sea and Baffin Bay suggests the two basins are characterized by different water mass endmembers (Pacific and Atlantic origins, respectively), with deep water DIC $\Delta^{14}C$ in Baffin Bay being significantly older than that of the Canada Basin.

Thesis Acknowledgements

Thank you. Thank you to all my colleagues, collaborators, family, and friends. This thesis could not have been completed without your unwavering support, and I am grateful for you.

First and foremost, I want to thank my supervisor, Dr. Brett Walker. Thank you, Brett, for investing so much of your trust in me. You didn't blink when I asked if I could follow my heart to the West Coast for the remainder of my thesis and I am so thankful for everything you've done to support me from afar. You funded my dreams and threw me on an airplane headed North (twice), so I can now proudly say I've sailed across the entirety of our country. Your genuine passion for science, teaching and superhuman multitasking abilities are inspirational, and I value the friendship we've cultivated over the years. I look forward to keeping in contact and wish you all the best in success after my degree.

Next, I wish to thank all the incredibly skilled and kind technicians I've been so fortunate to work with over these past few years. Thank you, Jennifer Walker, for your devoted teachings and analysis. You exceeded expectations to ensure I was properly trained for the task at hand, and you guarded my samples with your life, saving me from weeks of re-extractions with your highly attuned AMS-sorcery and strong inter-disciplinary management skills. I also owe Sr. Lab Technician and Instructor Kerry Klassen a huge debt of gratitude (and probably a coffee) for her bravery navigating illegally placed hot tubs and police checkpoints during the 2022 Canada Freedom Protest, just to ensure my samples were run on time. You are a legend, Kerry. I also thank you, Mr. Lab Manager Paul Middlestead, for guiding me around your prep space and billing my supervisor.

Our research could not have been conducted without the dedication of the entire Amundsen Science team and Coast Guard crew onboard and off the *CCGS Amundsen*. I thank you for the opportunity of a lifetime, your all-nighter shifts, your caring catering to the scientific community and your collaborative nature. Without you, a paper like this would be physically impossible.

Additionally, I want to thank our manuscript co-author Dr. Brent Else for his comments on our paper, his role as co-principal investigator during our 2021 RadCARBBS expedition and as Chief Scientist during our most recent (2023) expedition through Foxe Basin. I look forward to continuing our work together on our next methods paper.

Finally, I wish to thank a very special friend and past supervisor, Anthony Lapp. You, my dude, have helped me find my confidence and passion that proved invaluable over the course of this thesis. You always trusted me to get the job done right, and in much the same way as I have experienced with Dr. Walker, you have provided me with the scientific toolset I will carry with me for the rest of my life. I am very grateful for our friendship and for your constant encouragement of "are you done (your thesis) yet?".

Thank you to the entire uOttawa community, from profs to the department staff, for all the generous opportunities you've extended my way that have made me the scientist I am today. To my friends, family, and that special one in between, I appreciate you sticking with me throughout this entire process, and I love you all.

List of Figures

List of Tables

Glossary

AMS – Accelerator Mass Spectrometer

ANOVA – Analysis of Variance

AOU – Apparent Oxygen Utilization

ATL_{FS} – Atlantic Water Fram Strait

BBDW – Baffin Bay Deep Water

BIC – Baffin Island Current

CAA – Canadian Arctic Archipelago

C_{anth} – Anthropogenic Carbon

CBDW – Canada Basin Deep Water

CI – Confidence Interval

CTD – Conductivity, Temperature, Depth (probe)

DIC – Dissolved Inorganic Carbon

DOC – Dissolved Organic Carbon

$\delta^{13}C$ – Stable Carbon

$\Delta^{14}C$ – Radiocarbon

ETFE – Ethylene Tetrafluoroethylene

Fm – Fraction Modern

HDPE – High Density Polyethylene

IAEA – International Atomic Energy Agency

MW – Meteoric Water

NWP – Northwest Passage

pCO_2 – Partial Pressure of Carbon Dioxide

POC – Particulate Organic Carbon

PSW – Pacific Summer Water

PWW – Pacific Winter Water

SIM – Sea Ice Melt

SML – Seasonal Mixed Layer

UHP – Ultra High Purity

USGS – United States Geological Survey

WGIW – West Greenland Irminger Water

I. Literature Review

I.I Carbon Cycling in the Oceans and Controls on the Global Climate

Carbon is an essential element for life. CO_2 is the most abundant carbon gas molecule in the Earth's atmosphere and is disproportionately responsible for global climate change. Our climate is moderated by the Greenhouse effect, wherein molecules such as CO_2 and CH_4 absorb and reemit heat energy released by the Earth after warming from the Sun. Without it, the Earth's global average temperature would be 33°C cooler (World Meteorological Organization, 1982). Unlike many other common gasses in the atmosphere (e.g. N_2, O_2, Ar), CO_2 and CH_4 have large atomic structures that resonate at the same frequencies as the heat energy reemitted by the Earth, trapping heat like a greenhouse over the surface of our planet. Although water, another powerful and plentiful greenhouse gas, also resonates near these same frequencies, it has a considerably shorter residence time in the atmosphere (days versus millennia for CO_2) and is therefore less potent than CO_2.

Since the industrial revolution (~1750), human activity has drastically increased the amount of CO_2 in our atmosphere through the burning of fossil fuels, changes in land use and from chemical industrial processes such as concrete manufacturing. The carbon released by our actions is called "anthropogenic carbon". The present concern is that our anthropogenic carbon emissions will eventually overwhelm the Earth's natural carbon sinks responsible for moderating CO_2 in the atmosphere. Excess CO_2 in the atmosphere is expected to lead to climate warming on a global scale, and it is well accepted that continued global warming would lead to negative outcomes for humans and the environment; examples include rising sea levels, global loss of biodiversity, and increased socio-economic disparities. Unfortunately, there is evidence to suggest that the capacity

of the Earth's land and ocean carbon sinks are presently decreasing while the concentration of CO_2 in air is increasing (e.g. Le Quere et al., 2007). These large-scale climate interpretations remain debated, with some researchers suggesting the Earth's climate is managing itself (Knorr, W. 2009; Ballantyne et al., 2012; Sarmiento et al., 2014). Regardless, the potential impact of increased CO_2 levels in the atmosphere is significant and warrants further exploration.

The four major carbon reservoirs on Earth are: the hydrosphere, atmosphere, lithosphere and biosphere. Although the lithosphere contains orders of magnitude more carbon than any other reservoir, it cycles on geological timescales of hundreds of millions of years and more. The oceans are the largest actively cycling pool of carbon on Earth. Most carbon sequestered by the oceans is in the form of dissolved inorganic carbon (DIC; 38,000 GtC) through air-sea gas exchange and the "solubility pump". Here, gaseous CO_2 dissolves into the ocean and thermodynamically equilibrates with water to form carbonic acid, bicarbonate, and carbonate. The pH of the ocean determines speciation within the DIC equilibria, with carbonate acting to buffer carbonic acid and vice-versa. With an average pH of ~7.8, bicarbonate molecules are the most abundant. Depending on partial pressure differences between the atmosphere and ocean, CO_2 will either dissolve into sea water or be released into the atmosphere (Lueker et al., 2000). Once in the ocean, DIC is an essential carbon source for primary producers who fix DIC via photosynthesis. Living biomass and its by-products cover a wide range of particle sizes: dissolved organic carbon (DOC) constitutes the smaller end of the spectrum, including viruses, macromolecules, and colloids (all $<0.2\mu m$), while larger particulate organic carbon (POC) includes many bacteria, phytoplankton, and zooplankton ($\geq 0.45\mu m$). Collectively, DOC and POC contribute <700 PgC to the marine carbon pool (Schuur et al., 2016). POC sinking through the water column on time scales of days/months ("sinking POC") can sequester atmospheric CO_2 in deep sea sediments via the Biological Carbon Pump.

Smaller suspended POC can persist in the water column for over a decade (Bacon et al., 1987). DOC and POC are also central to the Microbial Carbon Pump, which can sequester carbon in the deep sea through the microbial transformation of labile organic matter to more recalcitrant forms (Jiao et al., 2010). In the deep ocean, slow heterotrophic remineralization of DOC and POC releases CO_2 back into the DIC pool on timescales of deep ocean circulation.

It is estimated that the global oceans have taken up nearly half of all anthropogenic emissions, while the global surface temperature has risen by 1.1°C since preindustrial times (IPCC 2023). To evaluate Earth's capacity to manage anthropogenic carbon emissions, we must first identify the carbon cycling mechanisms already in place and understand their limitations. Initiatives such as the Global Ocean Ship-Based Hydrographic Investigations Program (GO-SHIP) seek to do exactly this by coordinating fieldwork and amalgamating data from a multidisciplinary research community, centralizing topics in physical oceanography, the carbon cycle and marine biogeochemistry. Despite large monitoring programs such as this however, there exists comparatively less research conducted in the Canadian Arctic Archipelago (CAA). Often too, research there is conducted on a relatively smaller scale with less international funding. With the Arctic warming up to 4 times faster than the global average (Rantanen et al., 2022), the effects of melting permafrost, glaciers and sea ice on the marine carbon cycle remain unconstrained. Considering nearly half of the freshwater export from the Arctic Ocean passes through Baffin Bay on its way to the North Atlantic (Serreze et al., 2006), climate change in the Canadian Arctic has the potential to influence global thermohaline circulation if increased meltwater flux modifies North Atlantic deepwater formation. The consequences of this on global thermohaline circulation and the possibility of abrupt climate change remain poorly understood (Clark et al., 2002).

I.II DIC Concentrations, Stable Carbon, and Radiocarbon Isotopes as Tracers in the CAA

Analytical methods for DIC concentrations, alkalinity, pH and pCO_2 measurements are well established (Dickson et al., 2007). These data can be used to describe a variety of environmental processes such as seasonal shifts in carbon dynamics, to identify regions acting as sources/sinks of carbon, and/or for tracking terrestrial influences on marine ecosystems, among others. To make meaningful conclusions (e.g. detailed carbon budgets) with these data, a high spatial and temporal sampling resolution is required which can be difficult to conduct. Alternatively, combining DIC concentrations with isotopes such as stable carbon (^{13}C) and radiocarbon (^{14}C) can produce similarly diverse source interpretations without the need for repeat high temporal and (often) spatial resolution sampling.

98.9% of all natural carbon on Earth is stable in the form of ^{12}C; the remainder consists of heavier, stable ^{13}C (1.1%) and radioactive ^{14}C (10^{-7}%) isotopes. Natural processes such as weathering, photosynthesis, air-sea gas exchange and respiration selectively fractionate for or against different isotopes and their effects are well documented in literature. Reporting results as isotope ratios relative to ^{12}C ($^{13}C/^{12}C$ as $\delta^{13}C$ and $^{14}C/^{12}C$ as $\Delta^{14}C$) are then used to identify and interpret different processes by looking at the scale of their enrichments or depletions relative to expected global average concentrations. For example, Zeidan and coworkers (2022) used $\delta^{13}C$ and $\Delta^{14}C$ as estimators of anthropogenic carbon penetration in Baffin Bay. Fossil fuels are derived from ancient primary producers which fractionated against heavier ^{13}C and ^{14}C isotopes during photosynthesis, much like C3 plants do today. As a result, their diagenetic derivatives (natural gas, coal, oil, etc.) all have a depleted $\delta^{13}C$ of -20‰ or lower (IAEA, 2001). Also, since fossil fuels are significantly older than the half-life of ^{14}C ($\lambda = 5730$ years), $\Delta^{14}C$ values are radiocarbon dead (-1000‰) leading to a strong depletion of natural $\Delta^{14}C$ concentrations (~0‰) when combusted

and eventually incorporated into the marine carbon cycle or other systems. Similarly, Zeidan and coworkers (2022) investigated the depth of penetration of anthropogenic "bomb" carbon (+1000‰ $\Delta^{14}C$) produced from atmospheric thermonuclear bombs testing in the 1960s to estimate a residence time for Baffin Bay using $\Delta^{14}C$ radioactive decay and alkalinity proxies.

Although DIC $\delta^{13}C$ and $\Delta^{14}C$ are commonplace measurements for global ocean studies (ex. Bostok et al., 2010; Galbraith et al., 2015; Walker et al., 2008), few datasets exist in the Canadian Arctic. Griffith and coworkers (2012) present full depth DIC $\delta^{13}C$ and $\Delta^{14}C$ profiles for two stations in the Canada Basin within the Arctic Ocean that have yet to be reoccupied for DIC $\Delta^{14}C$. Similarly, Druffel and colleagues (2017) expand on this work with additional stations from multiple cruises within the Canada Basin measured for DIC $\Delta^{14}C$, however no repeat measurements have been made at these stations yet either. Bauch and coworkers (2015) present a comprehensive review of previously published DIC $\delta^{13}C$ values across the Arctic Ocean but coverage in the Canada Basin is minimal. It is obvious that there is a lack of largescale oceanographic DIC $\delta^{13}C$ and $\Delta^{14}C$ through the Canadian Arctic Archipelago (CAA). Other studies use more traditional DIC concentration measurements in CAA specific applications to fill this gap in the interim; examples include investigating how sea-ice algae blooms (ex. Else et al., 2019), arctic river drainage (ex. Brown et al., 2020) and variable sea-ice coverage (ex. Brown et al., 2015) affect DIC in the CAA. High-resolution physical oceanography transects and remote sensing have been used in combination with simulations and models to map the complex hydrography of the CAA (ex. Hughes et al., 2017), but there are less largescale biogeochemical data available to interface with these observations in a matter that concerns carbon cycling and climate change. A thorough study of nutrient flux through the CAA by Lehmann and coworkers (2022) also calls on this need for more biogeochemical data. Ultimately, Zeidan and colleagues (2022) provide the

most in-depth analysis of DIC isotope sources and cycling in the Canadian Arctic. We seek to expand this dataset across the CAA and Beaufort Sea to fill this fundamental knowledge gap. We discuss these data in the context of DIC biogeochemical processes in the Canadian Arctic which provide a baseline for future observations of global climate change.

I.III Overview of CAA Hydrography

The CAA is a complex ocean network of islands, ice, and water with uniquely diverse origins. Surface currents flow predominantly from West to East with fresher, lighter Pacific/Arctic waters following a steric drop of ~0.3m across the CAA to the Atlantic Ocean (Muench, 1970). Comparatively, the large shelf-to-basin ratio of the CAA severely restricts Eastward flow of deeper water masses and currents. Hypsometry data reveal that while all the World's Oceans and Seas combined have an average depth of 3729m, the CAA has an average depth of only 177m (Jakobsson, 2002). Studded with shallow sills and narrow gateways (e.g. Barrow Strait, through which all waters must flow: 125m deep and ~52km wide), water mass integrities and the halocline are broken by complex flows and counter flows, as well as tidal mixing and rotational hydraulics (McLaughlin et al, 2005). In regions with sea ice coverage, these features may also create open water polynyas. Shallow sills promote vertical mixing of warmer, nutrient-laden Pacific waters and resuspended sediment up to the surface, stunting sea ice formation, and creating a nursery for enhanced air-sea gas exchange, primary production and heterotrophy (e.g. Williams et al., 2018).

Pacific waters enter the Arctic Ocean from the Bering Strait and either advect into the Beaufort Sea immediately or navigate the shallow Chukchi and East Siberian shelves before joining the anticyclonic gyre in the central Canada Basin (Aagaard et al., 1981; Coachman & Barnes, 1961; Rudels et al., 1994). From here, these waters can hug the shelf current along the Southern Beaufort Sea and travel the Western edge of the CAA, percolating in through the many gateways on its way to Greenland (McLaughlin et al., 2005; Steele et al., 2004). Meanwhile,

denser, lower nutrient Atlantic waters enter the Artic Ocean through Fram Strait, between Greenland and Svalbard, or through the Barents Sea adjacent to Russia, the latter differentiated by higher nutrient/oxygen concentrations (McLaughlin et al., 2005). Similar to Pacific origin waters, the Atlantic branches may become entrained in the central Canada Basin gyre before being redistributed to the Northwestern CAA. Atlantic water also enters the CAA through Davies Strait in Southern Baffin Bay. Once inside, waters are expected to transit the CAA within 2 years (Tao & Myers, 2022). Despite this however, the unique hydrography of the archipelago contains numerous basins which may increase residence times. Examples include up to 13 years in the Kitikmeot (Williams et al., 2018), or 360-690 years in Baffin Bay (Zeidan et al., 2022). Once through, CAA modified waters enter the North Atlantic through either Davis Strait in the South of Baffin Bay, or via the Hudson Strait from Foxe Basin.

The freshwater character of the CAA is set by the dominance of relatively fresh Pacific/Arctic water, precipitation, riverine flux and variable, seasonal sea ice coverage. For example, we measured the average salinity in the Kitikmeot Sea at 27.5 across five entire water column profiles (max 282m), which is significantly lower than the average Arctic Ocean salinity reference value of 34.8 (Aagaard & Carmack, 1989). Unique within the CAA, this fresh, marine environment exhibits an estuarine-like circulation pattern where large volumes of freshwater input from a regional concentration of rivers mixes with deeper inflowing Pacific waters to produce low salinity outflow (Williams et al., 2018). Additionally, decadal observations note sea ice thickness has decreased significantly in the Kitikmeot (Howell et al., 2006), further exacerbating the freshwater budget. Net precipitation directly over the Arctic Ocean itself accounts for 24% of all freshwater input (Serreze et al., 2006). Combined, this makes the CAA the single largest exporter of freshwater to the North Atlantic (35%; Serreze et al., 2006). With significant sea ice and

freshwater export from nearby Fram Strait, an increase in Arctic Ocean freshwater input to the North Atlantic is likely to cause variability in deep water formation and global thermohaline circulation/climate (Serreze et al., 2006; Holland et al., 2001). Due to the shallow nature of the CAA, eustatic sea level rise associated with climate change will likely have a disproportionately large impact on this Arctic marine system.

1. Manuscript Submission

Tracing Pan-Canadian Arctic Water Masses and Anthropogenic Carbon Flux using Dissolved Inorganic Carbon Stable and Radiocarbon Isotopes

L. Jasperse[1], J. Walker[1], B. Else[2] and B. Walker[*1,3]

[1] Department of Earth and Environmental Science, University of Ottawa, Ottawa, ON, Canada.

[2] Department of Geography, University of Calgary, Calgary, AB, Canada.

[3] Department of Earth System Science, University of California, Irvine. Irvine, CA, USA.

*Corresponding author: Brett Walker (brett.walker@uci.edu)

Key Points

- Dissolved inorganic carbon ^{13}C and ^{14}C isotopes are effective tracers of water masses and carbon sources in the Canadian Arctic Archipelago and Baffin Bay.
- Negative ^{14}C values near the Mackenzie River show export of permafrost carbon, whereas "bomb" ^{14}C in the Kitikmeot region show modern terrestrial carbon.
- A comparison of historical ^{14}C depth profiles reveal significant uptake of fossil anthropogenic CO_2 in the Beaufort Sea over the past decade.

Abstract

The Canadian Arctic Archipelago (CAA) and Baffin Bay provide a direct connection between the Pacific, Arctic, and Atlantic Oceans. The Canadian Arctic is warming four times faster than the global average, yet the impact of this perturbation on the marine carbon cycle remains unknown. Dissolved inorganic carbon (DIC) stable isotope ($\delta^{13}C$) and radiocarbon ($\Delta^{14}C$) values are powerful tools for tracing water mass transport, residence times and carbon cycling. While the hydrography of the CAA is well documented, few DIC $\delta^{13}C$ and $\Delta^{14}C$ values exist for the region. Here, we present new DIC $\delta^{13}C$ and $\Delta^{14}C$ depth profiles from 19 stations across the CAA sampled in 2021 and place them into the context of 5 recently published Baffin Bay values. CAA DIC $\delta^{13}C$ and $\Delta^{14}C$ values ranged between -0.68‰ to +1.86‰, and -90.7 to +49.5‰, respectively. Several negative DIC $\Delta^{14}C$ values (-44.7‰ and -51.9‰) were observed near the Mackenzie River,

indicating riverine permafrost carbon is actively incorporated into the nearshore DIC pool. "Bomb" DIC $\Delta^{14}C$ values in the Kitikmeot Sea were attributed to enhanced tidal mixing and heterotrophy together with high regional water mass residence times. A comparison of historical DIC $\Delta^{14}C$ depth profiles reveals significant uptake of anthropogenic fossil CO_2 (via the Suess Effect) within Pacific Summer Water (PSW), Pacific Winter Water (PWW) and Atlantic Fram Strait Water (ATL_{FS}) in the Beaufort Sea. Finally, the contrast between deep Beaufort Sea and Baffin Bay DIC $\delta^{13}C$ and $\Delta^{14}C$ values reveal differences in residence time and carbon sources between the two regions.

2. Introduction

Marine dissolved inorganic carbon (DIC; 38,000Gt) is the ocean's largest carbon reservoir. Atmospheric CO_2 is effectively sequestered into marine DIC via air-sea gas exchange and the Solubility Pump. Heterotrophic remineralization of particulate organic carbon (POC; ~30GtC) and dissolved organic carbon (DOC; 662GtC) also contribute to the marine DIC pool, particularly in polar regions where air-sea gas exchange is limited by seasonal sea-ice extent (Shadwick et al., 2011). The surface oceans have a finite capacity for atmospheric CO_2 and yearly uptake rates are spatially variable (e.g. Landschützer et al., 2016). Anthropogenic fossil CO_2 emissions have altered the global climate and the marine carbon cycle, with approximately half of these emissions having been absorbed by the oceans (IPCC 2023). In-situ observations (e.g. Serreze & Francis, 2006; England et al., 2021), climate models (e.g. Holland & Bitz, 2003) and paleoclimate proxies (e.g. Park et al., 2019) all confirm that global warming is exacerbated in polar regions, with recent estimates suggesting the Arctic is warming up to 4 times faster than the global average (Rantanen et al., 2022). Meltwater flux through the Canadian Arctic Archipelago (CAA) has the potential to

influence global thermohaline circulation through freshening and increased stratification during North Atlantic deep water formation (Aagaard & Carmack, 1989, 1994).

The Arctic Ocean is currently thought to be a net carbon sink, with DIC uptake rates of $225 \pm 49 TgC\ yr^{-1}$ occurring primarily during the summer months (MacGilchrist et al., 2014). Within the CAA however, atmospheric CO_2 sequestration is less well constrained (e.g. Papakyriakou & Miller, 2011). A recent study by Beaupré-Laperrière and co-workers (2020) suggests that the Beaufort Sea and Queen Maud Gulf within the CAA are undersaturated with respect to aragonite and are both regions of net carbon uptake and acidification. Even so, a perennial sea-ice cover in much of the remaining CAA presents a logistical difficulty to take samples of sufficient spatial and temporal resolution to quantify pan-Arctic carbon fluxes using traditional pCO_2, alkalinity and DIC concentration measurements (e.g. MacGilchrist et al., 2014; Olsen et al., 2015). Instead, DIC stable carbon ($\delta^{13}C$) and radiocarbon ($\Delta^{14}C$) isotopes provide powerful tools for evaluating the carbon cycling while requiring less intensive sampling resolutions.

DIC $\delta^{13}C$ can be used as a carbon source indicator (for water masses) but can also undergo fractionation during biogeochemical processes such as CO_{2aq} acquisition by primary producers and/or heterotrophic respiration of POC. Contributions of anthropogenic fossil CO_2 emissions also affect the marine DIC pool, observable as highly negative $\delta^{13}C$ (-27‰) and $\Delta^{14}C$ (-1000‰) values. These negative isotope signatures are translated to marine and terrestrial biospheres (Guilderson et al., 2000; Reimer et al., 2004) and provide key evidence for anthropogenic carbon sequestration in the oceans via the Suess Effect (Revelle and Suess, 1957; Keeling, 1979; Körtzinger et al., 2003). "Bomb" $\Delta^{14}C$ values (+1000‰) produced from atmospheric thermonuclear bombs testing in the 1950s and 1960s have also been incorporated into the marine DIC pool. In the 1970's, DIC

$\Delta^{14}C$ values peaked in seawater at ~+200‰ but have since decreased to ~0‰ today due to ocean carbon uptake and the Suess effect (Mahadevan 2001). Some "bomb" DIC $\Delta^{14}C$ carbon remains in oceans gyres, at intermediate depths and in proximity to terrestrial systems.

Few DIC $\delta^{13}C$ and $\Delta^{14}C$ values have been published for the Arctic Ocean, and far fewer for Canadian Arctic regions. A wide range of deep DIC $\Delta^{14}C$ are reported, from -55‰ in the deep Eurasian Basin (Östlund et al., 1982), -141‰ in the deep Canada Basin (Östlund et al., 1987) and -90‰ in deep Baffin Bay (Zeidan et al., 2022), and have been used to estimate deep water residence times. Additionally, a few studies have observed a correspondence between DIC $\delta^{13}C$ values (with a 2-3‰ range) and Arctic water masses (Griffith et al., 2012; Zeidan et al. 2022). Here, we present a new high spatial resolution transect of DIC concentrations, $\delta^{13}C$ and $\Delta^{14}C$ data for the CAA and Pan-Canadian Arctic. We discuss these data in the context of water mass origins, advection, and biogeochemical processes together with previously published data from Baffin Bay (Zeidan et al., 2022). We also combine our data with historical Beaufort Sea DIC $\Delta^{14}C$ values to evaluate the depth and magnitudes of fossil fuel uptake via the Suess Effect.

3. Materials and Methods

3.1 Sample Collection

Seawater was sampled for DIC concentration, stable carbon ($\delta^{13}C$) and radiocarbon ($\Delta^{14}C$) isotopic analysis aboard the CCGS *Amundsen*. Full water column depth profiles were sampled from 19 stations in the CAA, from the Beaufort Sea to Lancaster Sound in 2021 (Cruise# 2104, Leg 4; Figure 1a,b). Additionally, we include samples from 5 out of 11 stations in Baffin Bay (Cruise #1902, Leg 2) collected in 2019 and previously reported by Zeidan and co-workers (2022). We used identical sample collection methods and analysis methods to those reported by Zeidan and co-workers and briefly summarize them herein.

Seawater was collected using a CTD rosette equipped with 24 Niskin bottles (12L) and a sensor array including a SBE 911plus conductivity, temperature, depth probe, oxygen, PAR, fluorescence, and transmissometer. DIC samples were collected directly from Niskin bottles into 250mL Pyrex bottles with 10% HCl cleaned polypropylene caps and ETFE pouring rings (Corning #1395-250). Bottles were pre-cleaned by first soaking in 10% HCl for a minimum of 1 hour. Acidified bottles and caps were rinsed with copious volumes of 18.2 MΩ Milli-Q water (total organic carbon <2ppb), dried and combusted at 540°C in a muffle furnace for 2 hours. Pre-cleaned (10% HCl) ultra-high purity silicone tubing was used to interface with the CTD rosette and to overfill each DIC sample from the bottom up with three times the bottle volume and capped. Care was taken to exclude air bubbles from the tubing and bottles during sampling. At least one DIC replicate sample bottle was taken from a random Niskin at each station (Table S2). Following collection, shipboard samples were opened in the aft chemistry lab, poisoned with 1 drop (50µL) of saturated $HgCl_2$, re-capped, mixed, and stored at room temperature in the dark.

3.2 DIC Concentrations and Stable Carbon Isotope ($\delta^{13}C$) Analysis

DIC samples were prepared following established methods for $\delta^{13}C$ analysis (Torres et al., 2005; Zeidan et al., 2022) and DIC concentrations (Olack et al., 2018). Sets of 5-6 DIC sample bottles were loaded at a time into a disposable glove bag alongside pre-cleaned (10% HCl, Milli-Q rinsed and 540°C/2h combusted) 12mL Exetainer® vials (Labco 938W) and caps (Labco VW101). The glove bag was purged a minimum of three times with ultra-high purity (UHP 5.0) Helium to ensure no atmospheric CO_2 contamination. DIC sample bottles were cracked ajar in the glove bag and loosely recapped, using hand tools (tongue and groove pliers) occasionally to aid in loosening tight caps. Next, 1mL of sample was pipetted into labelled Exetainer® vials and capped producing slight overpressure. An additional purge of the glove bag was performed halfway through sample splitting into Exetainer® vials to minimize possible contamination from previously

opened DIC sample bottles. Analytical replicates from the same sample bottle were taken every $n = 10$ samples. Helium glove bag "blanks" were also collected in Exetainer® vials at the end of each session to screen for atmospheric CO_2.

Isotopic standards with a suite of $\delta^{13}C$ values bracketing seawater DIC $\delta^{13}C$ ranges were prepared to ensure robust data accuracy, precision, and error propagation. International standards used include IAEA NBS-18 carbonatite with $\delta^{13}C = -5.01‰$; IAEA NBS-19 limestone with $\delta^{13}C = +1.95‰$; and USGS LSVEC lithium carbonate with $\delta^{13}C = -46.5‰$. Internal lab standards included sodium bicarbonate with a range of $\delta^{13}C$ values (VL-1 $\delta^{13}C = -3.21‰$; VL-2 $\delta^{13}C = -15.80‰$; VL-3 $\delta^{13}C = -13.89‰$) and calcite (C-44 with $\delta^{13}C = -1.85‰$) provided by the Ján Veizer Stable Isotope Laboratory at the University of Ottawa; OXG calcite standard with $\delta^{13}C = -7.5‰$ from Oxford University and CA-14 calcium carbonate $\delta^{13}C = -14.4‰$ (Sigma-Aldrich C4830-100G, lot #SLBD0293V) were also used.

Standards weighed directly into Exetainer® vials were flushed for a total of 4 times and capped in the glove bag following the procedure described above. Half of the standards were injected with 1mL of acidified and CO_2 stripped seawater to control for potential isotopic offsets between standards in pure acid vs. those acidified in 1mL of seawater. All samples and standards were acidified with 100µL of 85% H_3PO_4 (Fisher Chemical, HPLC grade, A260500), shaken and left to equilibrate with their headspace at room temperature for 12 hours prior to analysis. Samples were analyzed in the Ján Veizer Stable Isotope Laboratory using a Thermo-Finnigan Gas Bench (GB) coupled to a Thermo-Finnigan Delta V-Plus Continuous Flow Isotope-Ratio Mass Spectrometer (IRMS). Results are reported relative to the Vienna Pee Dee Belemnite (V-PDB) for $\delta^{13}C$ in the standard permille (‰) notation.

Standards percent carbon values and GB-IRMS peak areas were used to determine sample DIC concentrations. Here we applied partial least-squares calibration curves of measured standard peak area vs. mass of carbon acidified. Only peak areas from the first sample injection were used. The resulting calibration regression slope and intercept values were used calculate sample DIC concentrations using known extracted sample volumes in each Exetainer®. DIC concentration uncertainty based on n = 23 duplicate sample bottles was ±19µM. This agrees with a recent GB-IRMS study estimating uncertainties of ±1-2% (Olack et al., 2018). While this level of precision is much lower than individual measurement precision of DIC determined via coulometry (±1.1µM; Johnson et al., 1993), our total analytical error (±30µM) is only ~3.8 times higher than previous DIC inter-comparison studies using coulometry on sample replicates (±7.8µM; Zeidan et al., 2022) and thus reasonable to use for exploring broadscale shifts in DIC concentrations between Pan-Canadian water masses.

Replicate internal standards were spread evenly throughout each run allowing for time-based instrument drift corrections. Only one sample run required a minor drift correction where a statistically significant regression slope of standard $\delta^{13}C$ vs. time was observed. There, sample $\delta^{13}C$ values were corrected for "source stretching" using a partial least-squares linear regression of measured vs. known standard values (better than $R^2 = 0.9999$ for $n = 4$). The $\delta^{13}C$ analytical precision from sample and bottle replicates (n = 42), and standards (n = 123), was 0.05‰ and 0.09‰ respectively.

3.3 Radiocarbon Isotope ($\Delta^{14}C$) Analysis

DIC samples were prepared for $\Delta^{14}C$ analysis following a modified headspace CO_2 extraction technique (Gao et al. 2014; Zeidan et al., 2022). As for $\delta^{13}C$ analysis, all glassware used was pre-cleaned with 10% HCl, rinsed with Milli-Q water and combusted at 540°C/2h prior to use. Here, approximately 40mL of sample was decanted into pre-cleaned 60 mL glass vials (Fisher

Scientific #5719398) under an UHP (Grade 5.0) Nitrogen atmosphere in a disposable glove bag. Once subsampled, vials were immediately capped with a Viton septum (Supleco #27355) overlain by a PTFE lined silicon septum (Fisher Scientific 288-7222). Samples were then acidified with 0.5mL of 85% H_3PO_4 using a glass syringe (Hamilton #81520) equipped with a 23-gauge side port needle (Fisher Scientific #14815488) and reacted on a heat block for 2 hours at 75°C.

DIC secondary standards were prepared using two carbonate standards (University of California, Irvine Coral Standard, Fm = 0.9444 ± 0.0018; IAEA C2 travertine, Fm = 0.4114 ± 0.0003) and an in-house ^{14}C-free sodium bicarbonate (uOttawa $NaHCO_3$, Fm = 0.0000). Both "full size" (~1mgC) and "size-matched" (0.2 – 0.5mgC) standards were weighed into custom made 1.0 x 0.9cm cylindrical Pyrex cuvettes then placed in the glove bag. For each standard, approximately 40mL of pre-stripped seawater (Milli-Q with 1mL 85% H_3PO_4 per 100mL H_2O, bubbled with UHP N_2 for 15 minutes) was decanted into a 60mL glass vial in the N_2 glove bag. Standards were added to the 60mL acidified water vials by tilting the vial sideways, sliding the cuvette just inside, capping the vial, and then letting the standard powder in the cuvette fall into solution to begin reacting. Vials were then mixed and reacted on a heat block for 2 hours at 75°C and vortexed occasionally for conversion to CO_2.

The evolved headspace CO_2 was next cryogenically purified and manometrically quantified on a vacuum line, and flame-sealed into 9mm Pyrex tubes for graphitization following the sealed-tube Zinc method (Xu et al. 2007; Walker and Xu, 2019). DIC $\Delta^{14}C$ values were measured at the A.E. Lalonde AMS Laboratory at the University of Ottawa on an Ionplus AG Mini Carbon Dating System (MICADAS). Results reported here are corrected for year of collection and background subtraction with "size matched" modern and ^{14}C-free standards following the conventions set forth by Stuiver and Polach (1977). The average precision of replicate seawater

samples is better than ±2‰ (n = 20). For individual measurement data and precision, we refer the reader to Table S2.

4. Results

4.1 Seawater DIC Concentrations

The maximum DIC concentration measured in the CAA was 2.65 mmol L^{-1} and the minimum was 1.79 mmol L^{-1} (an ~860µM range; Figure 2a). At all stations, surface DIC concentrations within the seasonal mixed layer (SML; nominally ~40m depth) increase with increasing depth. At depths greater than 100m, DIC concentrations remained consistent. For example, at the three deepest stations in Baffin Bay (stations 193, BB2 and 224) DIC within the same water masses (Intermediate 300 to 1200m, Deep Water >1200m) were all within error of ±0.03 mmol L^{-1}. Stations 323 in Lancaster Sound and C012 in the Kitikmeot have variable concentrations with depth (±0.22 mmol L^{-1} and ±0.11 mmol L^{-1}, respectively) and a maximum between ~150-200m. Generally, we observe lower DIC concentrations in Baffin Bay (1.94 – 2.28 mmol L^{-1}) than in the CAA and Beaufort Sea (2.02 – 2.53 mmol L^{-1}), respectively. The lowest (1.79 mmol L^{-1}) and highest (2.65 mmol L^{-1}) DIC concentrations were observed at the surface of station 323 and bottom of the adjacent station C002 in Lancaster Sound, respectively. Overall, our reported DIC concentrations are consistent with previous work reporting DIC via coulometric methods in Baffin Bay (Zeidan et al., 2022), the CAA (Beaupré-Laperrière et al., 2020), and the Beaufort Sea (Miller et al., 2014).

4.2 DIC $\delta^{13}C$ Values

DIC $\delta^{13}C$ values had a 2.54‰ range across the CAA and Baffin Bay sample set; from -0.68‰ to 1.86‰ (n = 215; Figure 2b). The majority of $\delta^{13}C$ values above 200m were positive, ranging between +0.04‰ to +1.86‰ (n = 138), with only n = 4 samples having negative

$\delta^{13}C$ values between -0.02‰ to –0.68‰. DIC $\delta^{13}C$ values were the most positive in the surface and were more negative near ~200m depth. Surface samples from stations 434 and 476, adjacent to the Mackenzie River mouth, had the most negative $\delta^{13}C$ values (-0.68‰ and -0.35‰, respectively). Two deep (>1000m) stations in Baffin Bay (BB2, 224) had more negative $\delta^{13}C$ values (-0.16 to -0.68‰) than all other stations sampled (Figure 2b). The most negative DIC $\delta^{13}C$ value in deep Baffin Bay is -0.68‰ while the lowest value below 1000m in the Beaufort Sea was +0.89‰.

4.3 DIC $\Delta^{14}C$ Values

DIC $\Delta^{14}C$ values had a ~140‰ range across the CAA and Baffin Bay sample set; from -90.7‰ to 49.5‰ (n = 200; Figure 2c). We observe strictly positive $\Delta^{14}C$ values within the SML at 6 stations (0.4 to 20.9‰) in Baffin Bay (stations 193, 224 and BB2), the Kitikmeot region (C011, C012) and East of Bellot Strait (C003). The remaining 16 stations in the CAA and 108/323 had at least two negative SML DIC $\Delta^{14}C$ values (11.8 to -51.9‰). Stations 434 and 476, adjacent to the Mackenzie River outflow, had the lowest surface $\Delta^{14}C$ values observed in the study (-51.9 ‰ and -44.7‰ respectively; Figure 2c). Similar negative DIC $\Delta^{14}C$ values were only observed at >1000m depth in Baffin Bay and the Beaufort Sea. In general, we observe increasing DIC $\Delta^{14}C$ values with depth up to ~400m, with DIC $\Delta^{14}C$ values decreasing with depth thereafter. Station C004 is an exception to this trend, with a nearly constant $\Delta^{14}C$ depth profile (ranging between -0.2‰ and -9.1‰). It is also the only station with negative $\Delta^{14}C$ values at all depths. The two deep stations in Baffin Bay (224, BB2) have the most negative $\Delta^{14}C$ values in the dataset (Figure 2c).

5. Discussion

5.1 Hydrographic Setting: Water Masses in the Canadian Arctic Archipelago

The Northwest Passage (NWP) consists of a series of marine waterways connecting the Arctic and North Atlantic Oceans via the Canadian Arctic Archipelago (CAA), Baffin Bay and Hudson Strait. The hydrography of this region is unique and comprises wide ranges in surface salinity (18.4 to 33.5), sea surface temperature (–1.4 to 9.5°C), substantial river discharge and seasonal ice melt. Deepwater circulation is constrained by shallow sills and much of the shallow CAA experiences tidal mixing along continental shelves. For a detailed overview of the hydrography of the Canadian Arctic and the CAA, we refer the reader to McLaughlin et al., (2005). We briefly describe major current systems and water masses in the CAA and Baffin Bay below.

A seasonal mixed layer (SML; 0-40m depth) is present throughout the Canadian Arctic and is defined by low salinities ($S < 31$), a wide range of (generally warm) temperatures (-1.27 to 5.41°C), low nutrient concentrations (nitrate concentrations near 0) and maximum oxygen concentrations (Figure 3; Rudels et al., 1996; Yamamoto-Kawai et al., 2008). In the Western Canadian Arctic, cooler and less saline Pacific water enters the Chukchi and Beaufort Seas through the Bering Strait. Pacific water can be differentiated into two water masses with distinct temperatures and salinities that are attributed to their season of formation. Pacific Summer Water (PSW; 40-80m) is characterized by temperatures of -0.76 to -1.20°C, salinities of 31-32 and a density anomaly of σ_θ of 24.5 to 26 kg m^{-3} (Figure 3). Pacific Winter Water (PWW; 80-200m depth) is colder (-1.29°C) with a salinity of 33.1 and denser (σ_θ = ~26.6 kg m^{-3}) due to winter sea ice formation and brine rejection in the Chukchi Sea (Figure 3; Aagaard et al., 1981, Watanabe, 2011). The predominant flow of surface water through the CAA is West to East via Parry Channel into Baffin Bay via Lancaster Sound.

Below PSW and PWW, warmer, saltier, Atlantic Fram Strait water (ATL_{FS}; 200-1500m) is found in the Beaufort Sea (McLaughlin et al., 2005). ATL_{FS} waters have a deep temperature maximum of 0.8°C with S = 34.8 and σ_θ of ~27.9 kg m^{-3}, along with relatively depleted nutrient levels (Figure 3; Lehmann et al., 2022). Canada Basin Deep Water (CBDW) occupies the remainder of the water column (>1500m) in the Canada Basin with a salinity of 34.9 and temperatures around -0.3°C with σ_θ >28 kg m^{-3} (Figure 3; Granger et al., 2018; Timmermans et al., 2006). Both Pacific and Atlantic water masses are found in the CAA; within the Amundsen Gulf, M'Clure Strait, and into Lancaster Sound. However, the extension of ATL_{FS} is limited by shallow sills in Dolphin and Union Strait, and Barrow Strait (McLaughlin et al., 2005). Similarly, deeper Pacific water masses do not cross the shallow sills of the Kitikmeot region (Coronation Gulf and Queen Maud Gulf).

The Kitikmeot Sea region has an expansive shallow shelf that spans the regions between Coronation Gulf and Queen Maud Gulf. Two shallow sills bordering the sea to the West (Dolphin and Union Strait, 18m sill depth) and Northeast (Victoria Strait, 20-30m sill depth) severely restrict the inflow of PSW (Williams et al., 2018) and isolate its surface circulation from the rest of the CAA. The region is also known for its low primary production and high river input (Williams et al., 2018). Alkire and coworkers (2017) placed an estimated freshwater discharge rate of all smaller CAA rivers at approximately 260 km^3 yr^{-1} which is less than that of the Mackenzie River at 322 km^3 yr^{-1}. Comparatively, the Kitikmeot region itself is estimated to receive only 41 km^3 yr^{-1} of river water versus 256 km^3 yr^{-1} from inflowing Pacific waters (Brown et al., 2016). The Coppermine, Back, and Ellice rivers have the greatest discharges reported by Alkire and coworkers (2017), although numerous other smaller rivers are also known to influence the geochemistry of the region (Brown et al., 2020). Tidal, "estuarine-like" mixing between meteoric surface waters,

sea ice melt and some Pacific water results in outflow of low salinity water into the Amundsen Gulf and M'Clintock Channel and significant water column stratification (Williams et al., 2018).

Finally, in Baffin Bay, remnants of PWW entering via Lancaster Sound and Arctic water entering through the northern gateways transform into the cold (–1.6°C), fresh (S < 33.8) Baffin Island Current (BIC) at depths down to 300m and a core σ_θ between 27.5 to 27.6 kg m^{-3} (Figure 3; Münchow et al., 2015). West Greenland Irminger Water (WGIW) is found at intermediate depths in Eastern Baffin Bay and is distinguished by its warm (> 2°C), saline (S > 34.1) waters and a density anomaly of 27.3 to 28 kg m^{-3} (Figure 3; Curry et al., 2011). Baffin Bay Deep Water (BBDW) circulates within the basin at depths of 1200 to 1800m and can be identified by its core values of S = 34.5, T = 0°C and σ_θ >27.7 (Figure 3; Curry et al., 2011).

5.2 DIC Concentrations, $\delta^{13}C$ and $\Delta^{14}C$ as Tracers of Physical and Biological Processes

DIC $\delta^{13}C$ is a reliable water mass source tracer (Kroopnick, 1985). Similarly, DIC $\Delta^{14}C$ can be used as both a water mass tracer and to estimate water mass ventilation ages (Broecker et al., 1985). However, water mass DIC $\delta^{13}C$ and $\Delta^{14}C$ values are susceptible to modification during advection due to air-sea gas exchange, primary production, microbial respiration of POC and ^{14}C radioactive decay (Mook et al., 1974; Kroopnick, 1985; Zhang et al., 1995; Vargas et al., 2021). The addition of allochthonous DIC from sea ice melt, rivers, and precipitation, can also modify nearshore DIC $\delta^{13}C$ and $\Delta^{14}C$ values (e.g. Tamše et al., 2015). Here we evaluate Pan-Canadian Arctic depth distributions of DIC concentration, $\delta^{13}C$ and $\Delta^{14}C$ values to see if they can be used to identify water masses and to evaluate the physical and biological processes responsible for changes in DIC isotopes relative to endmember values (Table S3) throughout the CAA and Baffin Bay. For DIC concentrations, $\delta^{13}C$, and $\Delta^{14}C$ values, we first discuss Pan-Canadian surface and deep

distributions across the CAA and Baffin Bay Region. We also discuss DIC dynamics within PWW transiting the CAA via Parry Channel and within the unique Kitikmeot Sea region.

5.2.1 Surface DIC Concentrations and Isotope Distributions

Stations nearest the Mackenzie River (476, PCB12, 434, PCB07) had low salinities (18.4 to 28.2), a larger range in DIC $\delta^{13}C$ values (-0.68 to 1.06‰) and negative $\Delta^{14}C$ values (-51.9 to -15.1‰; Figure 4b,d,e). It is worth noting that the stations most influenced by the river plume (476 and 434) had the most negative DIC $\delta^{13}C$ and $\Delta^{14}C$ values (-0.35 and -0.68‰; -44.7 and -51.9‰, respectively) of any surface samples in in the Canadian Arctic, with surface DIC concentrations of 2.13 and 2.12 mmol L^{-1} (Figure 4c,d,e). These two stations were impacted by the Mackenzie River outflow yet had similar DIC concentrations to nearby stations (PCB12 and PCB07 = 2.13 and 2.26 mmol L^{-1}; Figure 4c). These concentrations were only slightly lower than in the Amundsen Gulf (414) and M'Clure Strait (515, 518) suggesting the Mackenzie River does not appreciably alter nearshore DIC concentrations but could impact nearshore DIC $\delta^{13}C$ and $\Delta^{14}C$ values if riverine DIC isotopic composition differed significantly. For example, previous studies report similar DIC concentrations both in the Mackenzie River and the Beaufort shelf (Mucci et al., 2010). A combined salinity and $\delta^{18}O$ mixing model (e.g. Letscher et al., 2011) suggests surface water from 476 and 434 are comprised of 49% and 44% river water endmember, respectively (Walker and O'Reilly *personal communication*). A simple isotopic mass balance assuming offshore seawater DIC $\Delta^{14}C$ = -15.9‰ (station 546, 3m) estimates that Mackenzie River has DIC $\Delta^{14}C$ values between -75 to -98‰ at station 476 and 434, respectively. These values are reasonable considering the predominance of permafrost in the Mackenzie River watershed and high volume of freshwater it delivers to the Beaufort shelf. Recent studies have observed extremely negative DOC and POC $\Delta^{14}C$ values up to -180‰ and -729‰ in the Mackenzie River (Campeau et al.,

2020). Thus, it is reasonable to assume the negative DIC $\delta^{13}C$ and $\Delta^{14}C$ values indicate a significant fraction of permafrost carbon is being microbially translated into the Mackenzie River and nearshore marine DIC pool via heterotrophic respiration (Mol et al., 2018).

Far from the influence of nearshore rivers, sea ice melt (SIM) within the Arctic Ocean leads to a colder (-1.42 to -0.94°C), less saline (23.64 to 28.43) SML in the Beaufort Sea and Shelf regions (Figure 4a,b). While DIC concentrations in the Beaufort Sea and M'Clure strait are broadly consistent with the rest of the CAA (Figure 4c), we observe distinct isotopic signatures at these locations. Station 546, in the Beaufort Sea was sampled at the southernmost extent of sea ice coverage and had a surface DIC $\delta^{13}C$ value of +0.83‰ and $\Delta^{14}C$ value of -15.9‰. Here, recirculating surface currents of the Canada Basin are likely mixing $\delta^{13}C$ enriched SIM with minor contributions of underlying PSW. We also observe high DIC $\delta^{13}C$ values in M'Clure Strait (+1.56 and +1.60‰ at stations 515 and 518, respectively). The effects of SIM on DIC can be variable; for example, an average of n = 73 meltwater DIC $\delta^{13}C$ values from an arctic ice core suggest an average DIC $\delta^{13}C$ value of +1.11‰ (Brown et al., 2015) for SIM. However, Bauch and co-workers (2015) found that SIM does not appreciably change DIC $\delta^{13}C$ in the SML, but rather variable sea ice coverage can lead to increasing DIC $\delta^{13}C$ values through enhanced primary production which preferentially removes isotopically "light" DIC $\delta^{13}C$. Openings in sea ice may allow for outgassing of underlying supersaturated waters that would also increase DIC $\delta^{13}C$ values. Alling and coworkers (2012) demonstrated this positive $\delta^{13}C$ signal can be preserved under sea ice over vast distances when they attributed high DIC $\delta^{13}C$ in the halocline of the Canada Basin to enrichment under variable sea ice coverage in East Siberian Sea. One plausible explanation of our data is that M'Clure Strait values may be indicative of allochthonous transport of waters that have experienced

enhanced air-sea gas exchange, primary productivity and/or variable sea ice coverage (e.g. the Chukchi Sea).

Beaufort Sea surface DIC $\Delta^{14}C$ values increase with proximity to the CAA. In the Amundsen Gulf $\Delta^{14}C$ = -3.1‰ (C014) and in M'Clure Strait $\Delta^{14}C$ = -5.6‰ (515). Negative surface DIC $\Delta^{14}C$ values within the Beaufort Sea could be attributed to either Arctic uptake of anthropogenic fossil fuel (e.g. the Suess Effect), remnant influx of riverine permafrost DIC, or a high ^{14}C reservoir age in the region (e.g. a higher relative flux of ^{14}C-depleted subsurface water). Surface waters advect into the Amundsen Gulf from the Beaufort Sea and return via shallow sills at Dolphin and Union Strait (Mclaughlin et al., 2005), alongside some estuarine-like outflow of fresher water from the Kitikmeot Sea (Williams et al., 2018). Thus, the higher DIC $\Delta^{14}C$ values observed within the Amundsen Gulf might be attributed to high DIC $\Delta^{14}C$ coming either from the Kitikmeot Sea or enhanced heterotrophic remineralization of POC. The latter would be consistent with previous observations of high fluorescence, excess nutrients (e.g. NO_3^-, PO_4^{3-} and $Si(OH)_4$) and lower O_2 concentrations relative to the Beaufort Sea (Tremblay et al., 2008).

DIC concentrations within the Kitikmeot Sea region are generally similar to the Amundsen Gulf and Beaufort Sea. However, we observe two stations with low DIC concentrations of 1.79 and 1.97 mmol L^{-1} for C013 and C011, respectively (Figure 4c), likely indicating these samples are impacted by riverine discharge (e.g. Coppermine River or local rivers in Cambridge Bay). Surface DIC in the Kitikmeot region have positive $\delta^{13}C$ values (+1.13 to +1.39‰) and $\Delta^{14}C$ values ranging from +0.4 to +7.8‰ (stations C010-C013, 312). The region is also known for its low primary production and stratification (Varela et al., 2013), however enhanced tidal mixing on adjacent sills has been observed to result in nutrient upwelling, and to increase heterotrophic remineralization of POC (Williams et al., 2018). We hypothesize the input of modern terrestrial

carbon from local rivers combined with the conversion of modern sedimentary POC containing "bomb" ^{14}C into the DIC pool largely explains these DIC isotopic trends. While annual rates of POC remineralization may be low, the long residence time of the Kitikmeot Sea (~13 years; Williams et al., 2018) relative to the CAA (<2 years; Tao and Myers, 2022) would allow for modern DIC with high $\delta^{13}C$ to accumulate.

Surface water transiting the CAA from West to East via Parry Channel also branches southward into M'Clintock Channel and Victoria Strait (312); returning to Parry Channel again via northward flow in the Eastern M'Clintok channel (C009) and Peel Sound (C004; Figure 1b). At stations C009 and C004 we observe low DIC concentrations (1.93 and 1.95 mmol L^{-1}) relative to the rest of the CAA (Figure 4c). However, DIC $\delta^{13}C$ values from stations C009 and C004 (+1.62‰ and +1.46‰, respectively) were much higher than in Victoria Strait (312: +1.24‰) and the Kitikmeot region (<1.4‰). In fact, these stations were far more similar to stations 515 and 518 $\delta^{13}C$ values which is consistent with the known predominant advection of surface waters containing Pacific nutrients and higher rates of primary production via Parry Channel into these regions (Lehmann et al., 2022). Surface DIC $\Delta^{14}C$ values for stations C009, 312 and C004 were modern (+0.5‰, -1.8‰, -4.3‰, respectively), and not dissimilar from central CAA values (Figure 4e).

Surface DIC $\delta^{13}C$ and $\Delta^{14}C$ values were similar within Prince Regent Inlet (C003; $\delta^{13}C$ = +1.80‰, $\Delta^{14}C$ = +2.6‰) and Lancaster Sound (C002 and 323; $\delta^{13}C$ = +1.70‰ and +1.49‰, $\Delta^{14}C$ = -0.8‰ and -1.5‰, respectively). Station C002 and C003 are located within a southerly surface current from Parry Channel and Lancaster Sound (Figure 1b). Modification of the DIC pool with southern advection into Prince Regent Inlet may impart small increases in DIC $\delta^{13}C$ (by +0.3‰) and $\Delta^{14}C$ values (by +4.1‰). This difference is significant, falling outside our total analytical

reproducibility for $\delta^{13}C$ and $\Delta^{14}C$ measurements (2σ = ±0.1‰ for $\delta^{13}C$, and better than ±4‰ for $\Delta^{14}C$). Increasing DIC $\delta^{13}C$ and $\Delta^{14}C$ values within Prince Regent Inlet could be the result of continued primary production with water mass advection which would enrich the residual DIC pool in $\delta^{13}C$ and add modern DIC $\Delta^{14}C$.

Surface DIC $\delta^{13}C$ and $\Delta^{14}C$ distributions have been previously reported for Baffin Bay (Zeidan et al., 2022). Here, changes in surface DIC $\delta^{13}C$ and $\Delta^{14}C$ were largely attributed to the influx of Atlantic waters via Davis Strait or Arctic Water via the Northern Gateways. Surface water in central Baffin Bay have low measured DIC $\delta^{13}C$ values of +0.69 to +1.14‰, while surface DIC near Greenland have higher DIC $\delta^{13}C$ values (~ +1.50‰). Similarly, surface Greenland waters have more positive $\Delta^{14}C$ values than in central Baffin Bay. Zeidan and co-workers (2022) attribute these trends to higher nutrient loading and rates of primary production near Greenland. However, at the time of publication only Atlantic DIC isotopic endmembers and a few Pacific samples were available (Griffith et al., 2012; Druffel et al., 2017), making isotopic linkages to the broader CAA region difficult to assess.

The continuity of available data spanning the CAA aid our interpretation of DIC concentrations, $\delta^{13}C$ and $\Delta^{14}C$ values in Baffin Bay. Surface DIC concentrations in the Northern Gateways and central Baffin Bay (1.96 ± 0.03 mmol L^{-1}; n = 5) were generally lower than much of the CAA (2.07 ± 0.13 mmol L^{-1}; n = 24) and also stations near Greenland (1.99 ± 0.08 mmol L^{-1}; n = 6). While the difference between the two average Baffin Bay station populations was not significant, individual stations have up to ±100µM offsets from West to East (Figure 4c). These results are consistent with previous studies observing export of low temperature and lower DIC Arctic Water in Western Baffin Bay within the BIC and a contrasting northern flow of higher temperature and DIC concentrated waters from the Atlantic via the West Greenland Current

(Zeidan et al., 2022; Azetsu-Scott et al., 2012). Similar DIC $\delta^{13}C$ and $\Delta^{14}C$ values found across Parry Channel (from stations 515/518 to 323) are strong indicators that DIC entering Baffin Bay via Lancaster Sound all have high $\delta^{13}C$ values and modern $\Delta^{14}C$ signatures (Figure 4d,e). Surface waters within Parry Channel and Lancaster Sound have similar temperature and DIC $\delta^{13}C$ values (within ±0.5°C, and ±0.10‰). Surface DIC $\Delta^{14}C$ values become more positive by >5‰ in Lancaster Sound perhaps due to heterotrophic remineralization of POC near Barrow Strait (Lehmann et al., 2022; section 4.2.3).

5.2.2 Sub-surface DIC Isotope Distributions Through the CAA and Baffin Bay

In this section, we discuss the distribution of DIC concentrations, $\delta^{13}C$ and $\Delta^{14}C$ values within water masses found in the Beaufort Sea, CAA and Baffin Bay (Figure 5a). We evaluate these data in the context of water mass origin, relative aging, biological activity, air-sea gas exchange, and meteoric water flux impacting the Pan-Canadian Arctic DIC pool. Below the SML, PSW (~40-80m; σ_θ = 24.5–26.0 kg m^{-3}) is the only water mass to span the entire CAA (Figure 5b). Previous studies corroborate these observations and have found Pacific water transits the CAA from M'Clure Strait to Barrow Strait via Parry Channel (i.e. The Deepwater Route) entering Baffin Bay through Lancaster Sound (Ingram and Prinsenberg, 1998; Jones et al., 2003, Lehmann et al., 2022). Some PSW enters the shallow Kitikmeot Sea region but is highly modified by freshwater input (Figure 5c; Williams et al., 2018).

DIC concentrations within PSW are variable across the CAA (2.24 to 2.56 mmol L^{-1}), but generally have lower concentrations in Baffin Bay (2.09 to 2.18 mmol L^{-1}). DIC $\delta^{13}C$ values decrease and $\Delta^{14}C$ values increase within PSW (Figure 5f,h) as it transits the CAA via both the Parry Channel but also in the southern CAA from the Amundsen Gulf to the Gulf of Boothia (e.g. from $\delta^{13}C$ = 1.58 to 0.59‰ and $\Delta^{14}C$ = -12.8 to 2.9‰, for stations 518 to C002, and 414 to C002

respectively). Enhanced air-sea gas exchange or riverine DIC flux does not appear to be principally responsible for these isotopic trends. Instead, changes in DIC $\delta^{13}C$ and $\Delta^{14}C$ PSW values are likely a product of changing biogeochemistry within the CAA. We hypothesize that heterotrophic remineralization of POC with negative $\delta^{13}C$ and positive $\Delta^{14}C$ values would thus simultaneously act to decrease DIC $\delta^{13}C$ values and increase resultant DIC $\Delta^{14}C$ values in the CAA. This is supported by previous studies observing the transport of macronutrients into the CAA via PSW that stimulates primary production on the Bering and Chukchi shelves (Codispoti et al., 2005; Sakshaug, 2004), and in the Amundsen Gulf (Forest et al., 2011; Tremblay et al., 2015; Sipler & Bronk, 2015; Shen et al., 2021). Enhanced POC remineralization at depth also results in increasing apparent oxygen utilization (AOU) in subsurface waters in the Amundsen Gulf and Western Lancaster Sound (Figure 5d), in support of the above interpretation.

With the exception of the Kitikmeot Sea region, PWW (80-200m; σ_θ = 26.0 – 27.0 kg m^{-3}) is present throughout the CAA. In the Beaufort Sea, PWW reaches a maximum depth of ~200m but shoals as it forms part of the BIC in Baffin Bay. We find PWW DIC $\delta^{13}C$ values increase from the West to East in the CAA (Figure 5f). PWW DIC $\delta^{13}C$ values in the Beaufort Sea (+0.16 ± 0.10‰; n = 14) are slightly lower than in Western Lancaster Sound and Prince Regent Inlet (C002, C003; +0.41 ± 0.10‰, n = 6). In Baffin Bay, DIC $\delta^{13}C$ values decrease to +0.19 ± 0.20‰ (n = 15) where PWW joins Arctic Water from Northern gateways to form the BIC. The added influence of fresh, cold Arctic Water in the BIC is also clearly reflected in a marked decrease in DIC concentration (e.g. from ~2.4-2.6 mmol L^{-1} in the CAA to ~2.12 mmol L^{-1} in the BIC; Figure 5e). Most striking, is the presence of increasing PWW DIC $\Delta^{14}C$ values from West (Beaufort Sea stations; -5.3 ± 11.2‰; n = 14) to East (C002, C003; +11.7 ± 4.5‰, n = 6) in the CAA and Baffin Bay (+13.9 ± 7.4‰, n = 15; Figure 5h). Increasing DIC $\Delta^{14}C$ advection of PWW across the CAA

and Baffin Bay could be attributed to either incorporation of atmospheric CO_2, continued flux of respired CO_2 from heterotrophic remineralization of POC, or continuous vertical mixing of deeper ATL_{FS} and WGIW DIC with higher $\Delta^{14}C$ values (Figure 5i). Apart from the Amundsen Gulf, we do not observe large increases in AOU within PWW along its generalized flow path. In addition, mechanisms for enhanced atmospheric CO_2 incorporation into PWW that would not also impact the SML and PSW are difficult to reconcile. Therefore, we hypothesize that vertical mixing/diffusion of deeper DIC with higher $\Delta^{14}C$ values (discussed below) is a more plausible mechanism for increasing PWW DIC $\Delta^{14}C$ across the Pan-Canadian Arctic. This mechanism is well established and has been used to reconcile the ^{14}C reservoir age of surface DIC in the global ocean (Koeve et al., 2015).

Beneath PWW, ATL_{FS} (200-1500m; σ_θ = 27.0–28.0 kg m^{-3}) is found at intermediate depths in the Canada Basin, Beaufort Sea, Amundsen Gulf and Parry Channel (Mclaughlin et al., 2005). Average ATL_{FS} DIC concentrations are high (2.49 ± 0.04 mmol L^{-1}, n = 20) but not significantly different than PWW values. Instead, we find significant increases in DIC $\delta^{13}C$ and $\Delta^{14}C$ values between PWW and ATL_{FS} (Figure 5g,i). Average ATL_{FS} has a DIC $\delta^{13}C$ value of +0.47 ± 0.23‰ and DIC $\Delta^{14}C$ of +31.5 ± 10.6‰ (n = 20) which, aside from the SML, are the highest subsurface DIC $\delta^{13}C$ and $\Delta^{14}C$ values observed in our study. We note that our Canada Basin DIC $\delta^{13}C$ and $\Delta^{14}C$ depth profiles have identical ATL_{FS} values to those previously published by Griffith et al., 2012 (Figure 7). These positive DIC $\delta^{13}C$ and $\Delta^{14}C$ values are a clear indication that Atlantic-origin (ATL_{FS}) "bomb ^{14}C" persists at these depths in the Canada Basin. Additional "bomb" carbon from the decay of modern, terrestrial organic matter delivered by rivers may increase this signal. At station 546, we have n = 1 sample representative of Canada Basin Deep Water (CBDW; >1500m; σ_θ >28.0 kg m^{-3}) which has a DIC $\delta^{13}C$ value of +1.05‰ and $\Delta^{14}C$ value of -60.3‰

is again consistent with previously published DIC $\delta^{13}C$ and $\Delta^{14}C$ values for aged CBDW (Griffith et al., 2012).

While subsurface DIC $\delta^{13}C$ and $\Delta^{14}C$ distributions were previously described for Baffin Bay (Zeidan et al., 2022), the continuity of Pan-Canadian data provide invaluable context for interpretation of DIC sources and cycling in Baffin Bay and its gateways. In Lancaster Sound and Baffin Bay, WGIW (200-1000m; σ_θ = 27.3–27.7 kg m^{-3}) is present at intermediate depths (Curry et al., 2011). While WGIW shares a similar regional origin to ATL_{FS}, it enters Baffin Bay via the Irminger Current which wraps around Southern Greenland (Figure 1a). Here it is heavily modified along its current extension on both the East and West coasts of Greenland (Curry et al., 2011), leading to distinct temperature/salinity properties and DIC isotopic composition from ATL_{FS}. For example, WGIW DIC concentration, $\delta^{13}C$, and $\Delta^{14}C$ values are much lower than ATL_{FS}, averaging 2.24 ± 0.13 mmol L^{-1}, -0.10 ± 0.15‰ and 5.8 ± 18.9‰ (n = 31), respectively. Baffin Bay depth profiles show progressive decreases in both DIC $\delta^{13}C$ and $\Delta^{14}C$ values with depth. Baffin Bay Deep Water (BBDW; >1200m; σ_θ >27.7 kg m^{-3}) has the lowest DIC $\delta^{13}C$ and $\Delta^{14}C$ values observed in the Pan-Canadian Arctic, averaging -0.39 ± 0.14‰ and -82.2 ± 8.5‰ (n = 9), respectively; Table S2). While BBDW DIC $\Delta^{14}C$ values are comparable to those values published for CBDW (-105 to -112‰; Östlund et al., 1987; Griffith et al., 2012), BBDW DIC $\delta^{13}C$ values are considerably more negative by ~1.5‰. Given these trends we suggest the most reasonable explanation for subsurface Baffin Bay DIC data is that distinct DIC sources from the Atlantic, together with long deep water residence times allow for enhanced DIC aging and changes in DIC $\delta^{13}C$ due to heterotrophic remineralization of isotopically "light" POC over exceptionally long timescales (Kroopnick, 1985; Emerson and Hedges, 2008). This interpretation would be consistent with published ^{14}C residence times for the region (360-690 years; Zeidan et al., 2022) but also the

elevated AOU values observed in BBDW (Figure 5d) and highlights the importance Baffin Bay plays in modulating Labrador Sea Water and Atlantic Meridional Overturning Circulation.

5.2.3 DIC Isotopic Shifts Within Parry Channel from M'Clure Strait to Lancaster Sound

Eastward currents transiting Parry Channel via M'Clure Strait (375m depth) enter Viscount Melville Sound (~550m; Mclaughlin et al., 2005) and later, Barrow Strait (125m), which restricts deep water masses (e.g. ATL_{FS}) from propagating further East into Lancaster Sound and Baffin Bay (>2000m; Mclaughlin et al., 2005; Lehmann et al., 2022). Here, we discuss possible mechanisms modifying DIC isotopic values along this route using two stations in M'Clure Strait (515, 518) and in Western Lancaster Sound (C002). We also place these changes into the context of past measurements reported from Baffin Bay (Zeidan et al., 2022). Before evaluating the modification of the DIC pool within Parry Channel, we first bin DIC data into specific water-masses using known water mass potential density ranges (SML, PSW, PWW; Table S3 and Figure 6a,b). A one-way analysis of variance (ANOVA) with a 90% confidence interval (CI) of σ_θ confirmed the presence of these water masses on either side of the Barrow Strait sill (Table S4). ANOVA tests (90% CI) of DIC concentrations, $\delta^{13}C$ and $\Delta^{14}C$ values suggest significant increases in DIC concentrations in PSW (Figure 6d), positive shifts in SML and PWW DIC $\delta^{13}C$ values, decreasing DIC $\delta^{13}C$ values in PSW, and positive DIC $\Delta^{14}C$ shifts in all water masses from West to East (Table S4). These isotopic shifts are readily observed in DIC isotope depth profiles (Figure 6e,f). The increase in DIC $\Delta^{14}C$ at all depths is interesting because the trend is not consistent with simple radioactive decay of ^{14}C and water mass aging with advection through the CAA. Instead $\Delta^{14}C$ values indicate either that DIC is becoming more modern as it transits Parry Channel, or that Lancaster Sound represents a distinct biogeochemical province from the Western CAA. Below we

discuss several possible mechanisms that contribute to our observed isotopic variations along the "Deepwater Route".

We have previously discussed the possibility of vertical diffusion of subsurface DIC with highly positive $\Delta^{14}C$ values as having the potential to modify PWW and PSW DIC $\Delta^{14}C$ values in the CAA. Using $\delta^{15}N$ and N* based tracers, Lehmann and co-workers (2022) proposed that diapycnal mixing between PWW and ATL_{FS}, as well as enhanced organic nitrogen remineralization (at depth), occur on either side of Barrow Strait. Additionally, Lavoie and co-workers (2005) observe weak vertical stratification in Barrow Strait and a vertical mixing of Pacific nutrients up to the surface. As such, the incorporation of ATL_{FS} DIC into PWW and PSW should increase DIC $\delta^{13}C$ and $\Delta^{14}C$ across the CAA. As mentioned above, we observe positive increases in DIC $\delta^{13}C$ for SML and PWW and positive increases in DIC $\Delta^{14}C$ for all water masses. Despite a small negative change in DIC $\delta^{13}C$ by -0.62‰ for PSW, the isotopic trends for all other water masses are consistent with vertical mixing of ATL_{FS} into shallower water masses over Barrow Strait.

An alternate interpretation would be the incorporation of modern or "bomb" POC $\Delta^{14}C$ into the DIC pool via heterotrophic remineralization within the SML, PSW and PWW between M'Clure Strait and Lancaster Sound. Recently measured POC $\Delta^{14}C$ values were very negative in M'Clure Strait (-59 ± 15‰ and -141 ± 12‰ for 515, 518), but far more positive POC $\Delta^{14}C$ values were observed in Western and Eastern Lancaster Sound (+13 ± 14‰ and -12 ± 9‰ for C002, 323; Fox and Walker, 2022; Zeidan et al., 2022). However, a simple isotopic mass balance suggests that between 1.7-1.8 mmol L^{-1} (66-69%) of respired POC CO_2 with $\Delta^{14}C$ = +13‰ would need to be added to raise DIC $\Delta^{14}C$ values from their maximal depletion (-16.9 and -19.5‰ at 100m in stations 515, 518) to the observed 100m DIC $\Delta^{14}C$ value at C002 (+2.9‰). This does not appear

to be conceivable given transit times across the CAA are at maximum 2 years (Tao and Myers, 2022).

Another possibility is that the sharp division in DIC biogeochemical provinces between Baffin Bay and the CAA could be due to a larger proportion of recently ventilated Arctic water contributing to water flux over Barrow Strait in Lancaster Sound than the advection of PSW and PWW. This could help explain some of our observed DIC $\delta^{13}C$ and $\Delta^{14}C$ isotopic trends, like the markedly lower AOU <200m at Baffin Bay influenced station C002 (Figure 6c); this likely reflects more recently ventilated Arctic water as opposed to the strict presence of PSW and PWW at these stations. Such an interpretation is not fully consistent with established physical oceanography of the region showing net advection of PSW and PWW from the West CAA to East CAA and into Baffin Bay (Mclaughlin 2005; Tao and Myers, 2022). While the remineralization of POC within PSW and PWW could add some DIC across Barrow Strait, our data do not appear to confirm this as a major process. Instead, tidally-driven mixing of ATL_{FS} water into shallower water masses over the sill in Barrow Strait and/or the presence of distinct biogeochemical provinces on either side of Barrow Strait seem more likely. These proposed mechanisms are readily testable. The observance of these isotopic shifts clearly highlights a need for further study. In particular, higher spatial resolution sampling of DIC isotopes (and marine organic carbon) should be performed within Parry Channel and on either side of Barrow Strait.

5.2.4 DIC biogeochemistry in the Kitikmeot Sea

With residence times of ~13 years (Brown et al. 2016), the Kitikmeot Sea is isolated from physical circulation relative to the rest of the CAA. Here, we briefly describe DIC concentration and isotopic trends in this oligotrophic, low primary productivity ecosystem (Williams et al., 2018). DIC concentrations in the shallow Kitikmeot Sea (2.20 ± 0.10 mmol L^{-1}; n = 18) are lower

than those in adjacent CAA regions. Based on tilting isopycnals in the region, it is clearly impacted by tidally-driven downward mixing extending to the seafloor from the influx of meteoric water from rivers such as the Coppermine, Burnside, and Ellice. Mixing models also suggest a net inflow of sea ice leads to significant meltwater contributions equivalent to one third of riverine input to the region, and strong near-surface stratification due to spring freshet peaking in August (Xu et al., 2021 and Afsharipour et al., 2023). At station C012, DIC $\delta^{13}C$ and $\Delta^{14}C$ surface samples have positive values (+1.39‰ and +7.8‰, respectively). DIC $\delta^{13}C$ gradually declines with depth to a minimum of +0.37‰, however we observe an overall increase in DIC $\Delta^{14}C$ (to +19.7‰) at a depth of 282m. Kitikmeot surface DIC $\delta^{13}C$ values are generally consistent with SML endmember values influenced by enhanced air-sea gas exchange, but also by the delivery of modern and "bomb" ^{14}C from rivers. At depth, we hypothesize that enhanced heterotrophic respiration of POC could be responsible for the observance of "bomb" ^{14}C in the deep Kitikmeot DIC pool. At the time of sampling, the region was nearing the end of its short ice-free season (July to October; Shen et al., 2021), thus the seasonal accumulation of pCO_2 from remineralized sinking POC is again consistent with our measured DIC $\Delta^{14}C$ and $\delta^{13}C$ values. It is also consistent with recent work observing high respiration and remineralization of nitrate at depth due to tidal mixing adjacent to sills in the region (Back et al., 2021), the presence of "bomb" ^{14}C in POC from the deep chlorophyll max (Fox and Walker, unpublished data) and the aforementioned Kitikmeot Sea residence time which would allow for regional persistence of "bomb" ^{14}C.

5.3 Constraining the "Suess Effect" and Rates of Anthropogenic Carbon Penetration in the Arctic Ocean Between 2009-2021

Early work reporting DIC $\Delta^{14}C$ values from the Arctic Ocean helped establish principal residence times of CBDW (500-800 years) in the Canada Basin (Östlund et al., 1987; Schlosser et

al., 1997). More recently, Griffith and co-workers (2012) reported DIC $\delta^{13}C$ and $\Delta^{14}C$ values from two Canada Basin stations in 2009, later expanded upon by Druffel and coworkers (2017) reporting DIC $\Delta^{14}C$ values from 8 stations in the Beaufort Sea and Amundsen Gulf (collected in 2012). Here we use recent changes in DIC $\Delta^{14}C$ values to evaluate the "Suess Effect" by quantifying rates of anthropogenic carbon (C_{anth}; $\Delta^{14}C$ = -1000‰) uptake into SML, PSW, PWW and ATL_{FS} DIC in the Canada Basin.

With the exception of station CB4, all stations shown in Figure 7a are within the same geographical area (~200km). We note that, to date, repeat sampling of these individual stations for DIC $\Delta^{14}C$ has not been performed. To evaluate the Suess Effect, we first assign DIC $\Delta^{14}C$ values to SML, PSW, PWW, ATL_{FS} water masses by matching CTD potential density (σ_θ) values to known endmembers (Table S3: Figure 7b). Water mass designations were subsequently confirmed by one-way ANOVA analysis of σ_θ to the 95% CI (Table S4). One-way ANOVA tests also confirmed statistically significant differences in DIC $\Delta^{14}C$ values (95% CI; Table S4) over the historical period between 2009, 2012 and 2021 for SML, PSW, and ATL_{FS}. A one-way ANOVA test for PWW DIC $\Delta^{14}C$ values fell just outside the 90% CI when comparing all sample years (n = 8). However, a comparison of 2009 to 2021 data are within 90% CI and we consider this to be statistically significant for the purposes of quantifying the Suess Effect.

Changes in DIC $\Delta^{14}C$ depth profiles from three of our Beaufort Sea stations (546, 434, 414), station CB4 from Griffith et al, (2012) and three stations (A98, H64, H49) from Druffel et al., (2017) are shown in Figure 7c. Here, we observe a consistent trend of increasingly negative DIC $\Delta^{14}C$ from 2009, 2012 and 2021 within SML, PSW and PWW. Excluding n = 1 highly negative DIC $\Delta^{14}C$ value from station 434 (2m) influenced by the Mackenzie River, DIC $\Delta^{14}C$ values from the SML (0-40m) had a 29‰ range, decreasing from $\Delta^{14}C$ = +19‰ in 2009, to +3‰

in 2012, and to an average of -10.3 ± 4.0‰ (n = 6) in 2021. Similarly, PSW (40-80m) DIC $\Delta^{14}C$ values decreased from +41.5‰ in 2009, to +3.2‰ in 2012 and had an average value of -10.9 ± 2.8‰ (n = 2) in 2021. In PWW (80-200m), DIC $\Delta^{14}C$ values decrease from +24.1‰ in 2009, to an average of 0.9 ± 2.7‰ (n = 2) in 2012 and an average of -8.0 ± 13‰ (n = 5) in 2021. These observed changes in DIC $\Delta^{14}C$ cannot be explained by radioactive decay of ^{14}C given the timescale of sampling (12 years). Instead, we attribute these DIC $\Delta^{14}C$ changes to the incorporation of fossil fuel CO_2 (C_{anth}; $\Delta^{14}C$ = -1000‰) into these respective Arctic water masses via the Suess Effect. Thus, historical DIC $\Delta^{14}C$ depth profiles represent the combination of modern and fossil CO_2 introduced via air-sea gas exchange, together with the vertical diffusion and mixing of deep water masses of distinct surface origin.

We also observe a negative DIC $\Delta^{14}C$ offset within ATL_{FS} between station A98 (Druffel et al., 2017; sampled 2009) and station 546 (2021; Figure 7c). Here, DIC $\Delta^{14}C$ values decrease from an average value of +49.3 ± 25.3‰ (n = 4) in 2009, to +36.6‰ in 2012 and an average of +22.5 ± 26.5‰ (n = 8) in 2021. However, an offset was not observed between our data and the offshore Canada Basin (CB4; sampled 2008) DIC $\Delta^{14}C$ depth profile reported by Griffith et al. (2012), complicating the interpretation of the Suess Effect within ATL_{FS}. One possibility for the lack of a $\Delta^{14}C$ change between the 2008 and 2021 profile (CB4 and 546) is coincidental, and that if CB4 were re-sampled today its DIC $\Delta^{14}C$ depth profile would be negatively offset from that previously reported due to the continued impact of the Suess Effect. Another possibility is that an offshore DIC $\Delta^{14}C$ gradient may exist within the Beaufort Sea, where nearshore stations are more strongly affected by riverine or shelf-born delivery of fossil allochthonous carbon (e.g. permafrost carbon or remineralized sedimentary organic carbon on shelves). Below 1500m depth, all three datasets (2008, 2009, 2021) have nearly identical DIC $\Delta^{14}C$ values, suggesting that the variance

observed in the upper water column (ignoring CB4) is real, and not an artifact of systemic differences between studies. While discrepancies in historical ATL_{FS} DIC $\Delta^{14}C$ are difficult to reconcile, they do not exclude the potential for the Suess Effect at depth in our study area and provide strong rationale for the future sampling of DIC $\Delta^{14}C$ at higher spatial resolution within the Canada Basin. In the meantime, A98 from 2009 represents a better point of comparison to our station 546 (Druffel et al., 2017).

Given the apparent incorporation of C_{anth} within SML, PSW, PWW and possibly ATL_{FS} DIC $\Delta^{14}C$ (Figure 7c), we next quantify C_{anth} concentrations, incorporation rates and masses of C_{anth} within each water mass. First, we use a simple isotopic mass balance together with Beaufort Sea hypsometry data (Jakobsson 2002) to quantify the fraction of C_{anth} (f_{Canth}) present in each water mass from the two historical periods (2009-2012 and 2012-2021) as well as over the entire period from 2009-2021 (*equation 1*).

$$(1)\quad f_{meas}\Delta^{14}C_{meas} = f_Y\Delta^{14}C_{Y1} + f_{Canth}\Delta^{14}C_{Canth}$$

Where $f_{meas} = f_Y + f_{Canth} = 1.0$, and f_Y is the year of comparison (e.g. 2009 or 2012), and $\Delta^{14}C_{meas}$ is the average DIC $\Delta^{14}C$ value for each water mass in 2021. $\Delta^{14}C_{Canth}$ is assumed to be -1000‰. Next, concentrations of $[DIC]_{Canth}$ (µmol L^{-1}) were calculated following *equation 2*.

$$(2)\ [DIC]_{Canth} = [DIC]_{avg}f_{Canth}$$

Where $[DIC]_{avg}$ is the average DIC concentration of our 2021 measurements within a water mass. Rates of $[DIC]_{Canth}$ (µmol L^{-1} y^{-1}) accumulation within water masses were estimated by dividing $[DIC]_{Canth}$ by the time period in question using *equation 3*.

$$(3)\ rate = \frac{[DIC]_{Canth}}{Year\ 2 - Year\ 1}$$

Based on the fraction of ^{14}C-free DIC needed to reproduce the observed DIC $\Delta^{14}C$ decrease, we estimate total C_{anth} additions between 2009-2021 to be 64.4 ± 4.8, 69.6 ± 2.4, 49.2 ± 1.9 and 61.6 ± 4.1 μmol L^{-1} for SML, PSW, PWW and ATL_{FS}, respectively. By binning the data into two historical periods (2009-2012 and 2012-2021) we find rates of C_{anth} accumulation are also decreasing. For example, rates of C_{anth} within the SML, PSW, PWW and ATL_{FS} were three to eight times higher between 2009-2012 (11.7, 28.9, 11.9, and 9.8 μmol L^{-1} y^{-1}) than between 2012-2021 (3.3, 3.7, 1.6, and 3.7 μmol L^{-1} y^{-1} respectively). Given observations of Arctic sea-ice decline, warming, freshwater delivery and stratification (Tremblay et al., 2015) and clear increases in anthropogenic fossil emissions (IPCC 2023), decreasing Suess Effect rates could indicate the Beaufort Sea is becoming saturated in CO_2 due to ocean acidification. This hypothesis agrees with numerous studies observing pCO_2 increases in the Canada Basin associated with sea ice loss, suggesting the Arctic Ocean is becoming less of a net carbon sink (Else et al., 2013; Ouyang et al., 2020; DeGrandpre et al., 2020). Alternatively, we suggest enhanced stratification due to Arctic freshening could be limiting vertical mixing and the penetration of atmospheric CO_2 to PSW, PWW and ATL_{FS}.

Nevertheless, these results suggest significant quantities of C_{anth} have entered the Beaufort Sea over the past decade. Using our determined added C_{anth} concentrations from 2009-2021 in conjunction with recent Beaufort Sea hypsometry and volume estimates (634 km^3; Jakobsson 2002), we determined the size of the C_{anth} reservoir for each Beaufort Sea water mass since 2009. These first order calculations would suggest that a total of 12.4 ± 1.1, 11.7 ± 0.7, and 21.9 ± 1.4 Tg C_{anth} have been added to the SML, PSW, and PWW, respectively for a total of 45.9 ± 1.9 Tg C_{anth} in the Beaufort Sea. Including estimated C_{anth} within ATL_{FS} (as estimated from the A98

profile), would add an additional 228.6 ± 19.0 Tg C_{anth} to the Beaufort Sea since 2009, further highlighting the importance of repeat hydrographic sampling of this region for DIC $\Delta^{14}C$.

6. Summary and Implications

Air-sea gas exchange, solubility, primary production and deep ocean heterotrophy principally influence DIC biogeochemistry (Sarmiento, 2006). Global warming has reduced Arctic seasonal sea ice extent (MacGilchrist et al., 2014; Rantanen et al., 2022). Increased freshwater input from melting sea ice, glaciers and rivers may act to further stratify the CAA, limiting vertical mixing and surface nutrient flux (Tremblay et al., 2015). Warming combined with uptake of pCO_2 via air-sea gas exchange leads to ocean acidification and changes in community composition (Azetsu-Scott et al., 2010; Ardyna & Arrigo, 2020; Beaupré-Laperrière et al., 2020). Despite these changes, our understanding of how the Arctic carbon cycle will respond to these perturbations remains poorly constrained. In this study, we show that DIC $\delta^{13}C$ and $\Delta^{14}C$ are effective transient tracers for identifying water masses and DIC biogeochemical processes in the Canadian Arctic. Our results provide critical baseline $\delta^{13}C$ and $\Delta^{14}C$ data for the Pan-Canadian Arctic and reveal a mosaic of biogeochemical provinces across the Beaufort Sea, CAA, and Baffin Bay. Exceedingly low DIC $\Delta^{14}C$ values in the SML adjacent to the Mackenzie River plume indicate the export of permafrost carbon is readily translated into the marine DIC pool and is observed up to 60km offshore. This observation is consistent with increased delivery of terrigenous organics from permafrost melting combined with enhanced wind-driven mixing strongly influencing the SML (McGuire et al., 2009; Mathis et al., 2012). Positive DIC $\delta^{13}C$ and "bomb" $\Delta^{14}C$ in the Kitikmeot Sea are consistent with a region dominated by riverine carbon flux, low primary productivity, estuarine-like flow, diapycnal mixing and net heterotrophy. DIC $\Delta^{14}C$ depth profiles suggests waters residing in deep Baffin Bay are significantly older than those of the Canada Basin, and the

stark contrast in DIC $\delta^{13}C$ values between the two regions highlight an Atlantic vs. Pacific origin for the two basins, respectively. A comparison of historical data within the Beaufort Sea suggests significant quantities of fossil C_{anth} have been incorporated, possibly to 1500m depth, and that rates of C_{anth} uptake are decreasing. Future work focused on producing higher resolution Arctic DIC isotope transects and the re-occupation of historical stations will greatly improve our ability to understand Arctic DIC biogeochemistry in a period of unprecedented global change.

7. Acknowledgments

We thank Chief Scientist Martine Lizotte, Anissa Merzouk, Alexandre Forest and the staff of *Amundsen Science*, the crew of the CCGS *Amundsen,* Aislinn Fox, and Kayla McKee for their help in supporting the field expedition and seawater sampling. We also thank the staff of the André E. Lalonde National Accelerator Mass Spectrometry Facility and the Ján Veizer Stable Isotope lab at the University of Ottawa for their support. This work was funded by an NSERC CGSM Scholarship (to L.J.), the Natural Sciences and Engineering Research Council (NSERC) of Canada through a Discovery Grant, Accelerator and Launch Supplements (RGPIN-2020-06501, RGPAS-2020-00071, DGECR-202000256; to B.D.W., RGPIN-2015-4780), a NSERC Discovery Grants Program – Shiptime grant (RGPST-544991-2020; Radiocarbon Distributions and Carbon Cycling between Baffin Bay and the Beaufort Sea (RADCARBBS) to B.D.W. and B.G.T.E), the New Frontiers in Research Fund (NFRFE-2019-00794 to B.D.W.) and the Canada Research Chairs program (CRC-2018-00050 to B.D.W.). This work is a contribution to ArcticNet, funded in part by the Networks of Centres of Excellence Canada, NSERC, the Canadian Institute of Health Research, and the Social Sciences and Humanities Research Council.

Conflict of Interest

The authors declare no conflicts of interest relevant to this study.

Data Availability Statement

The original contributions presented in the study are included in the article/Supplementary Material. Further inquiries can be directed to the corresponding author.

8. Figures with Captions

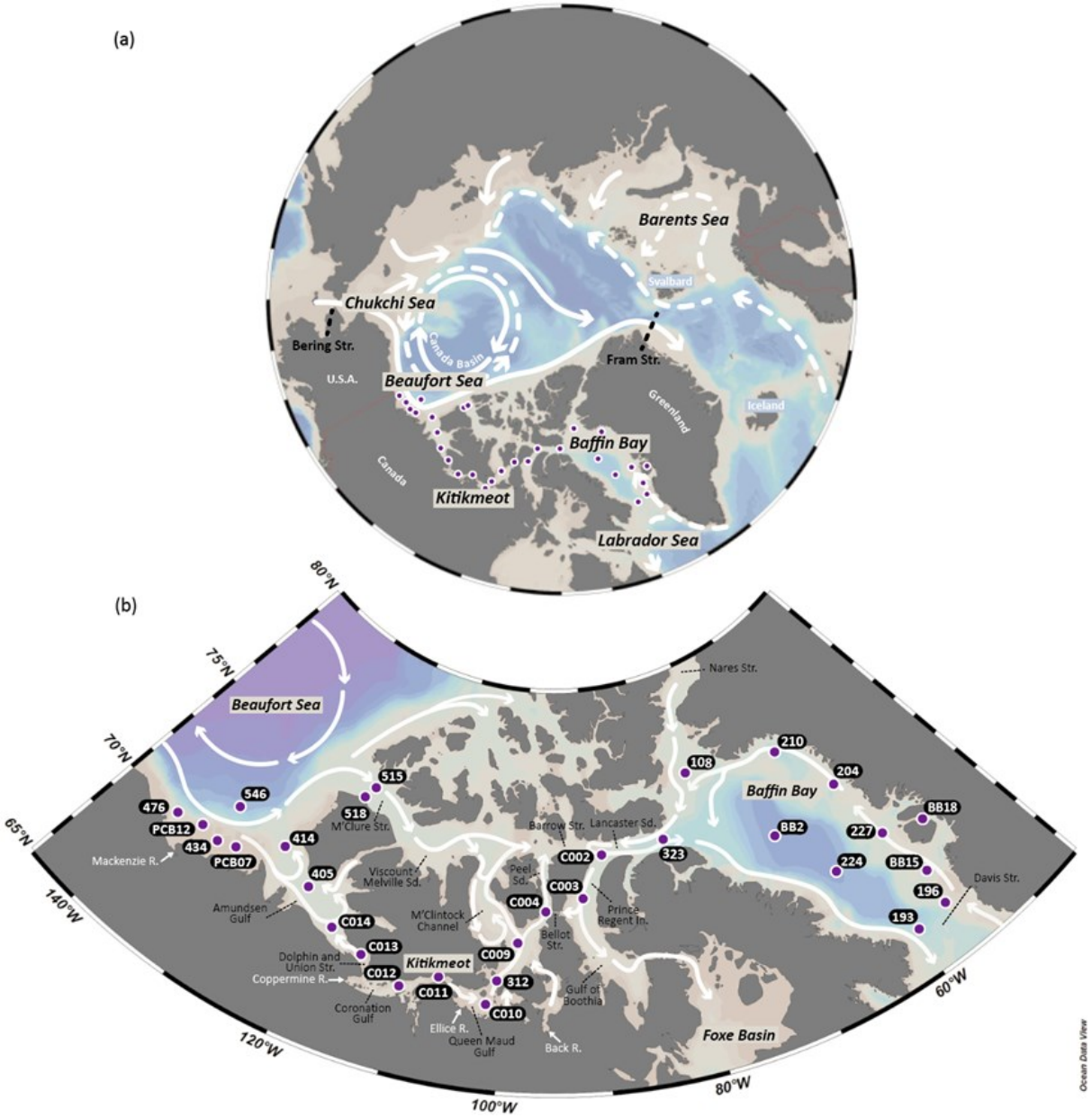

Figure 1. Seawater sampling locations within the Canadian Arctic Archipelago (CAA) and Baffin Bay. Purple dots represent sample locations with names written in black bubbles. In panel (a), solid white arrows indicate mean surface circulation patterns and dashed arrows represent intermediate depth circulation patterns in the central Arctic Ocean adapted from Lehmann et al., (2022). Panel (b) shows mean surface circulation patterns in the CAA adapted from Ingram and Prinsenberg (1998) relative to stations sampled during the 2019 Baffin Bay and 2021 RadCARBBS expeditions. Black text indicates important straits, regions and gateways, with white text identifying important rivers. Beaufort Sea, Baffin Bay and the Kitikmeot are three key basins providing water to the CAA. Station coordinates are available in Table S1.

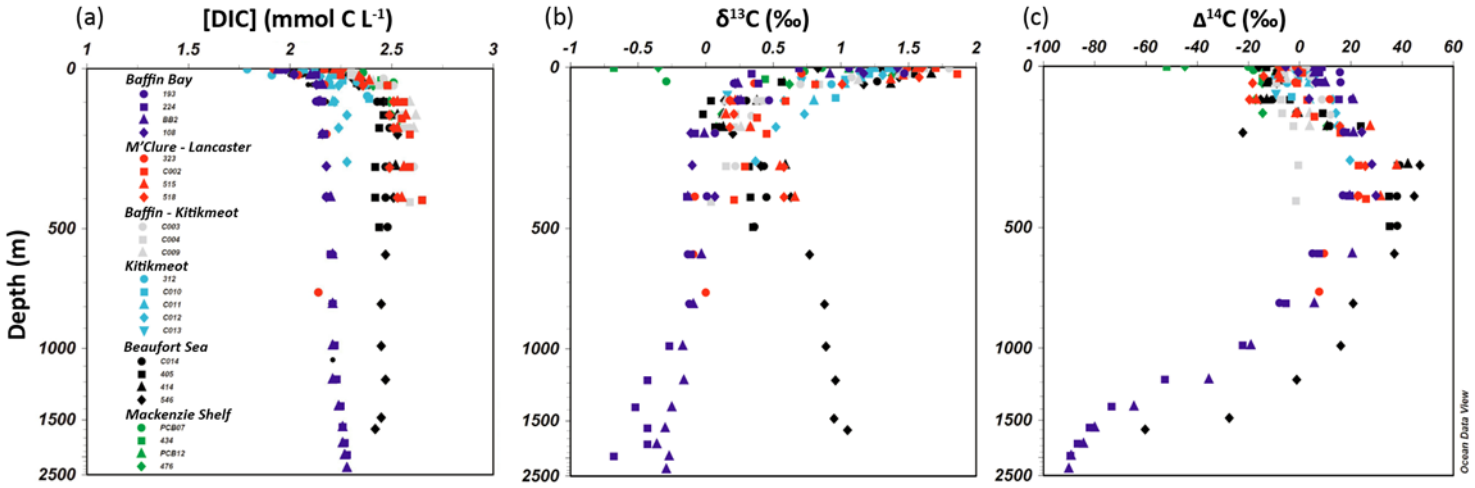

Figure 2. Depth profiles of DIC concentrations, $\delta^{13}C$ and $\Delta^{14}C$ values in the Canadian Arctic Archipelago. (a) measured DIC concentrations, precision ±0.03 mmol L^{-1} (b) measured DIC $\delta^{13}C$ values, precision = ±0.05‰. (c) measured age-corrected DIC $\Delta^{14}C$ values, precision better than ±2‰ (see section 2.3). Results plotted against temperature/salinity available in supplementary info (Figure S1).

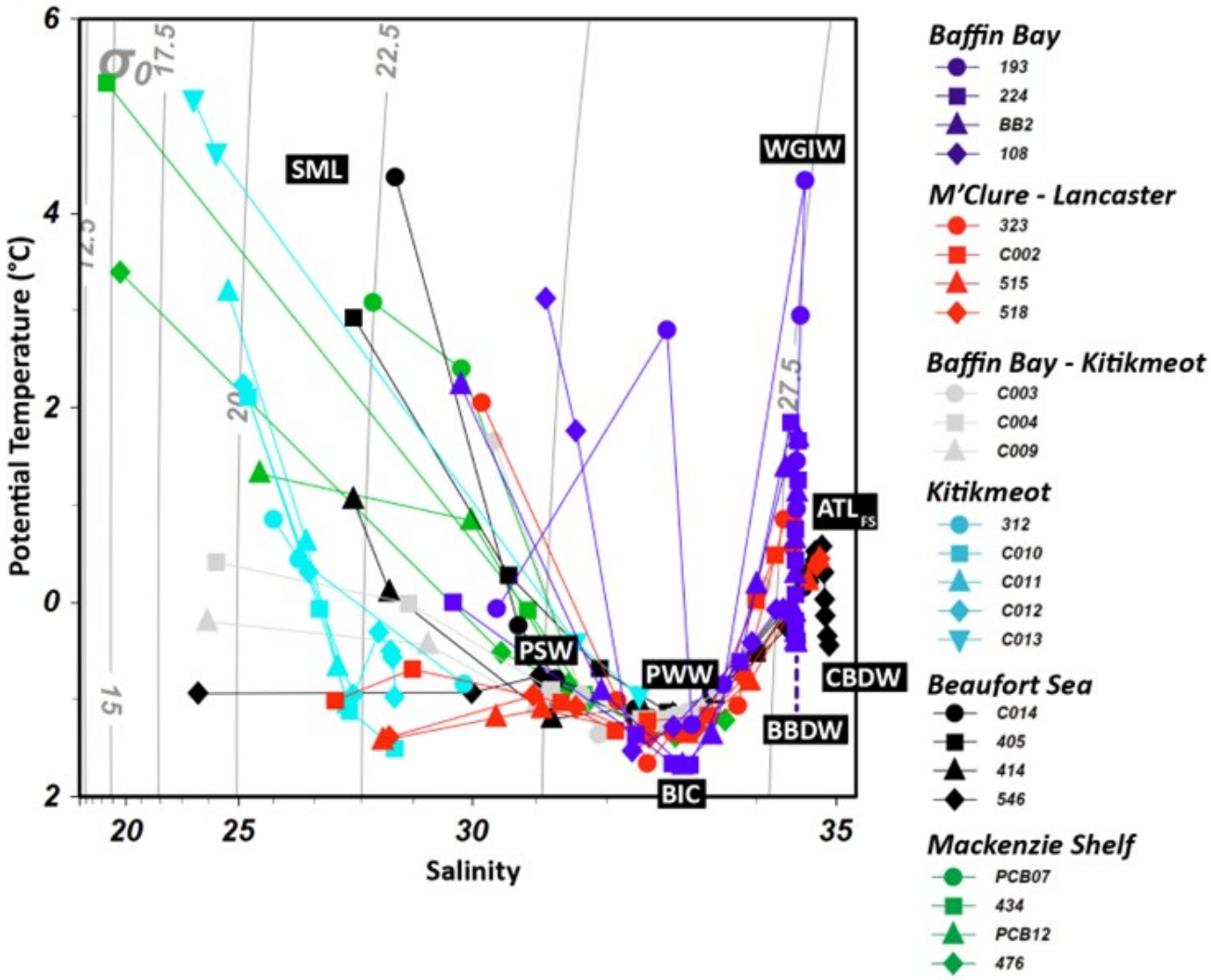

Figure 3. Potential temperature-salinity diagram for samples collected throughout Baffin Bay and the Canadian Arctic Archipelago. Water mass endmembers are presented as white text in a black box and include the Seasonal Mixed Layer (SML), Pacific Summer Water (PSW), Pacific Winter Water (PWW), Baffin Island Current (BIC), West Greenland Irminger Water (WGIW), Atlantic Water Fram Strait (ATL_{FS}), Canada Basin Deep Water (CBDW) and Baffin Bay Deep Water (BBDW). Solid grey lines show potential density anomaly contours measured as σ_θ in kg m^{-3}.

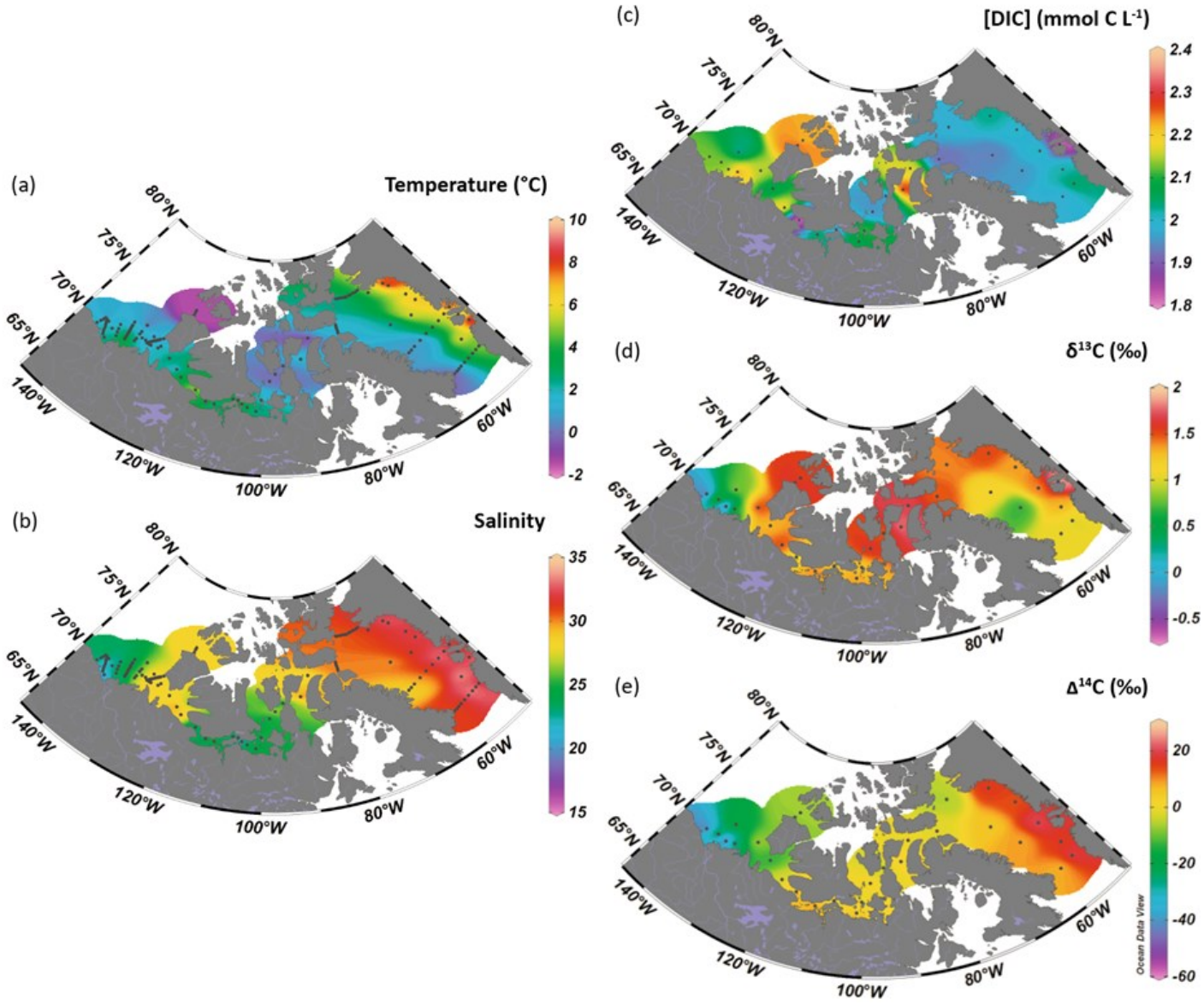

Figure 4. Surface distributions of physical water properties and DIC isotopes in the CAA (nominally shallower than 20m). (a) Surface CTD temperature values, (b) Surface CTD salinity values, (c) measured surface DIC concentrations, (d) measured surface DIC $\delta^{13}C$ and (e) measured surface age corrected DIC $\Delta^{14}C$ values. Black dots represent sample station locations with high resolution CTD data plotted only in (a) and (b).

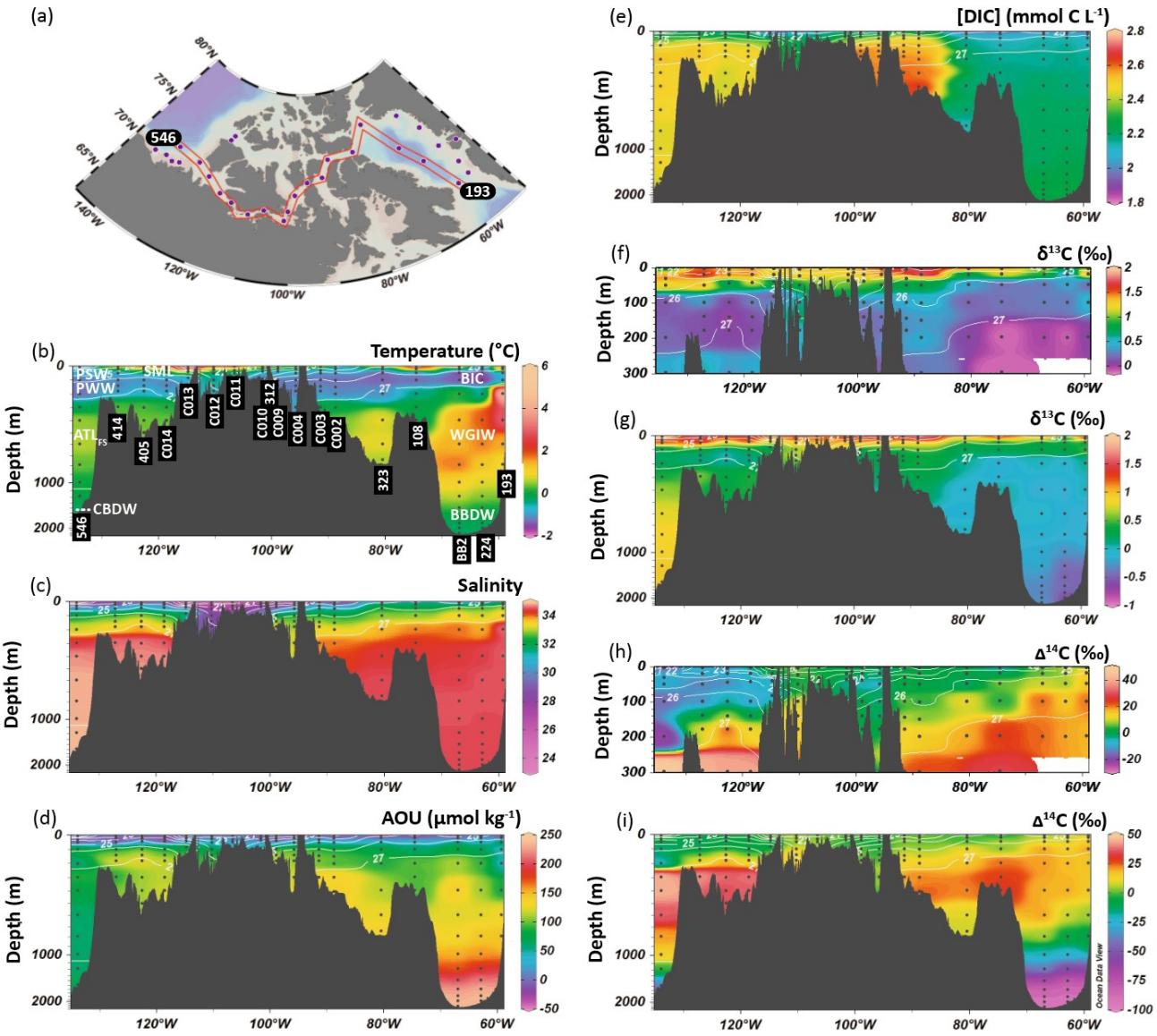

Figure 5. Section plots of DIC concentrations, isotopes and water properties in the CAA. Transect extends from the Beaufort Sea to Baffin Bay following path illustrated in (a) and stations listed in (b). Sample depths and locations are indicated by black dots. (a) map of transect stations through the CAA, (b) CTD temperature versus depth, (c) CTD salinity versus depth, (d) calculated apparent oxygen utilization (AOU) versus depth, (e) measured DIC concentration versus depth, (f) measured $\delta^{13}C$ versus depth for upper 300m, (g) measured $\delta^{13}C$ versus depth, (h) age-corrected $\Delta^{14}C$ versus depth for upper 300m, and (i) age-corrected $\Delta^{14}C$ versus depth. Solid white lines are potential density anomaly contours (σ_θ in kg m^{-3}). Water masses are labelled with white text and follow abbreviations in Figure 3.

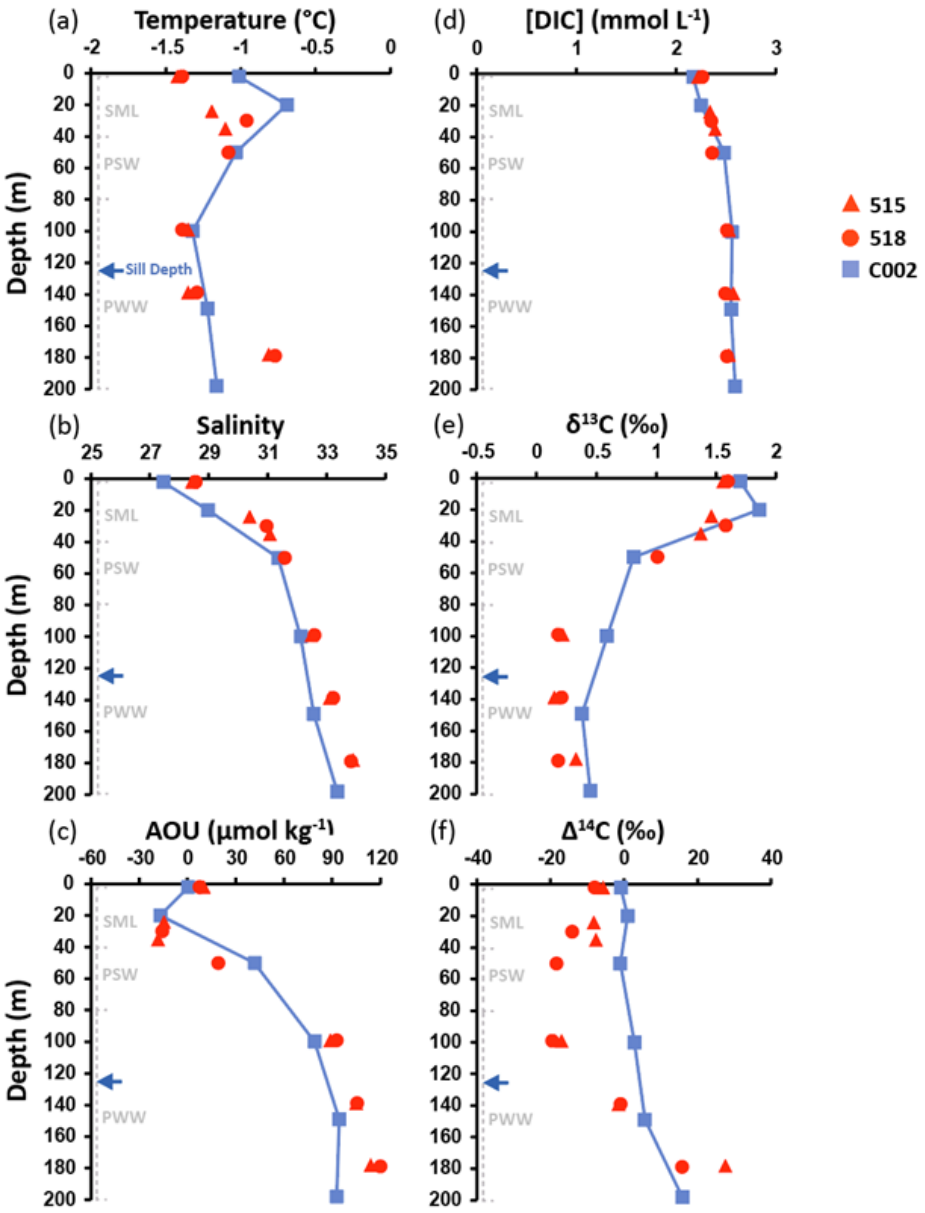

Figure 6. Depth profiles of hydrographic properties, DIC concentrations and isotopic values between M'Clure Strait and Lancaster Sound. For all plots, the blue arrow indicates the Barrow Strait sill depth (~125m). Dotted grey brackets represent approximate water mass depths for the Seasonal Mixed Layer (SML), Pacific Summer Water (PSW), and Pacific Winter Water (PWW). Red symbols represent stations in the West (M'Clure Strait) and blue in the East (Lancaster Sound).

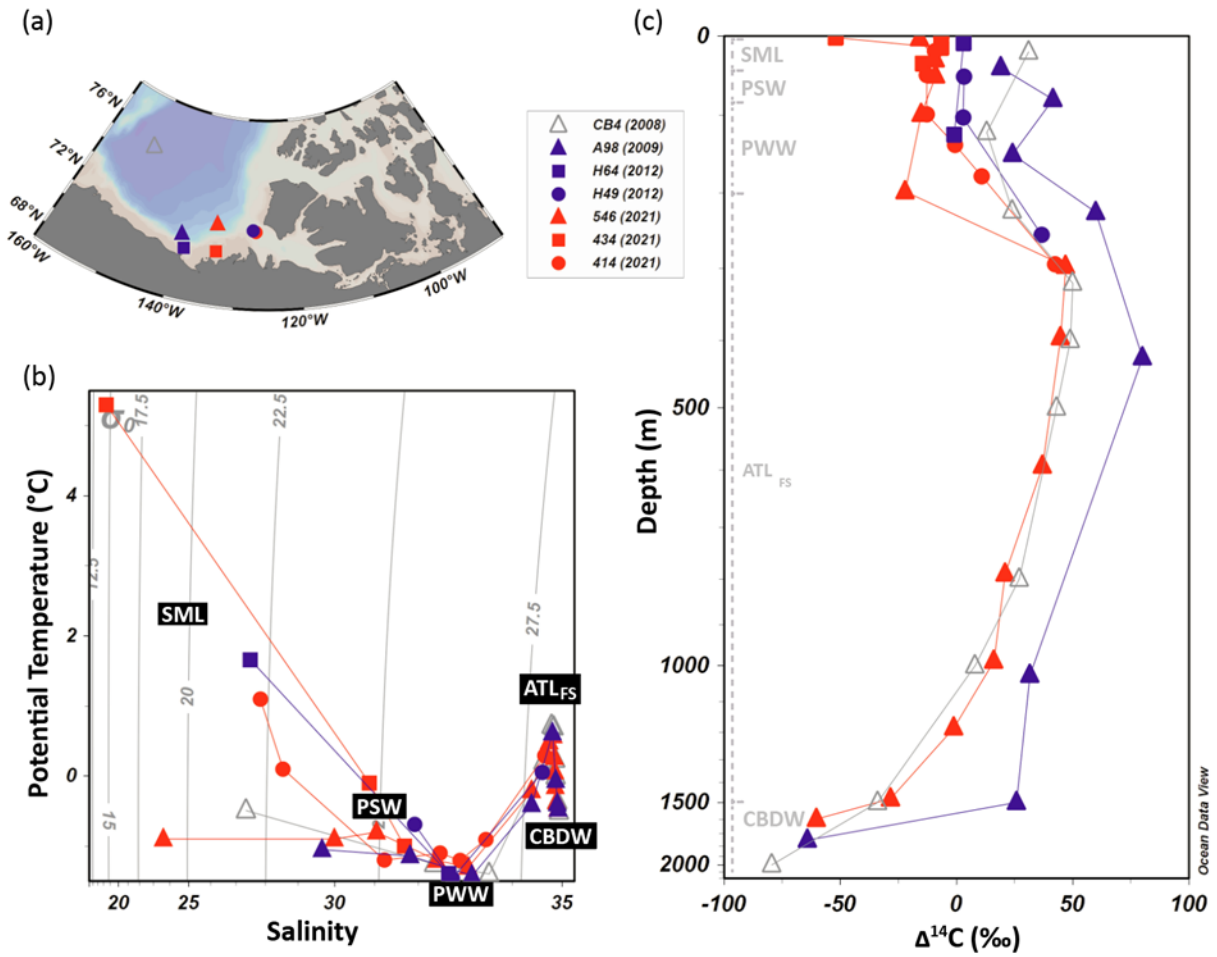

Figure 7. Beaufort Sea water masses and DIC $\Delta^{14}C$ depth profiles sampled between 2008 and 2021. Symbols are grey: Griffith et al., 2012, blue: Druffel et al., 2017, red: this study. (a) map of stations in the Canadian Arctic Archipelago and one station in the Canada Basin (CB4: 75°N and 150°W). (b) Potential temperature versus salinity plot showing water mass endmembers (following Figure 3) and density anomaly isopycnals (σ_θ in kg m^{-3}). (c) depth profiles of measured DIC $\Delta^{14}C$ and water mass depth ranges indicated by dashed grey brackets with grey labels. Individual measurement errors are ±4‰ for historical (2008-2012) stations and ±2‰ for our study. Dotted grey brackets represent approximate water mass depths for the Seasonal Mixed Layer (SML), Pacific Summer Water (PSW), Pacific Winter Water (PWW), Atlantic Water Fram Strait (ATL_{FS}) and Canada Basin Deep Water (CBDW).

9. Conclusions

Human activities have altered the Earth's carbon cycle. Global greenhouse gas emissions (most notably CO_2) continue to rise year by year, with polar amplification expected to warm the Arctic up to four times faster than the global average (England et al., 2021; Holland & Bitz, 2003; Park et al., 2019; Rantanen et al., 2022; Serreze & Francis, 2006). Warming poles lead to melting icecaps, and in turn, rising sea levels. Approximately 3.3 to 3.6 billion people, statistically those who have contributed the least to climate change, live in the most affected regions (IPCC 2023). Rising sea levels cause flooding, increase extreme weather event frequencies (e.g. droughts, heatwaves, cyclones and heavy rainfall), and can inflict severe damage on the human/natural environment (including reduced food/water security and loss of biodiversity/habitats). These are heavy consequences, yet the current state of our understanding of the Arctic carbon cycle remains inadequate (McGuire et al., 2009). Even poorer is our understanding of carbon dynamics in the CAA. Observations made thus far indicate that global warming and a reduced sea ice cover has made the Arctic Ocean a net sink for atmospheric CO_2 (Bates et al., 2006). Yet, net uptake rates of CO_2 as DIC have been observed to be decreasing in the world's oceans (e.g. Le Quere et al., 2007). With DIC accounting for more than 98% of all carbon in the global oceans, understanding its extant cycling mechanisms in the face of a rapidly changing global climate and melting Arctic is paramount. This thesis provides new, high-resolution DIC data along a vast transect through the CAA, from Baffin Bay to the Beaufort Sea, the likes of which are interpreted herein and are critical baseline data for which to compare future studies.

We use DIC concentrations, $\delta^{13}C$, and $\Delta^{14}C$ to identify large-scale biogeochemical processes modifying water masses transiting through the CAA. Our values had a wide range, from 1.79 to 2.65 mmol L^{-1}, -0.68 to +1.86‰, and -90.7 to +49.5‰ for DIC concentrations, $\delta^{13}C$, and

$\Delta^{14}C$ respectively. PSW was the only water mass we observe spanning the entirety of our transect, and it showed a general trend of decreasing DIC concentrations and $\delta^{13}C$ values and increasing $\Delta^{14}C$ from West to East. We attribute these shifts to differences in biogeochemistry across the CAA, largely due to heterotrophic remineralization of modern bomb carbon-containing riverine influx at intermediate depths. It is difficult to generalize trends throughout the CAA however, due to the numerous distinct biogeochemical provinces observed within. Two stations nearest the Mackenzie River plume had overwhelmingly negative DIC $\Delta^{14}C$ surface values consistent with previous studies reporting ^{14}C-deplete DOC/POC riverine export. Our data suggest ancient permafrost carbon is being microbially translated to the Arctic DIC pool. We observe distinct biogeochemical provinces in M'Clure Strait and Western Lancaster Sound, separated by Parry Channel, and we propose vertical mixing of ATL_{FS} over Barrow Strait may be responsible for the isotopic shifts. This hypothesis cannot be confirmed by our limited data set however, and so we highlight the need for the community to generate more data in this region. The Kitikmeot Sea is also identified as having its own distinct biogeochemistry, dominated by low DIC concentrations and positive isotopes due to concentrated freshwater input, relatively longer residence times and limited tidally driven upwelling at shallow sills bordering the region. At deep water depths, we use DIC $\delta^{13}C$, and $\Delta^{14}C$ to confirm Baffin Bay has its own distinct Atlantic water mass endmembers that are different from the Atlantic endmember in the Western CAA. We also identify SIM, air-sea gas exchange, riverine influx, tidal mixing, and heterotrophic respiration as important processes affecting DIC and carbon cycling in the CAA. Lastly, we use what limited historical DIC $\Delta^{14}C$ data available to quantify the Suess effect in the Beaufort Sea. Our results suggest this region of the Arctic Ocean has sequestered up to 275 Tg C_{anth} down to depths as deep as 1500m since 2009, but our evidence implies uptake rates are slowing.

DIC concentrations, $\delta^{13}C$, and $\Delta^{14}C$ are powerful tracers of physical, chemical, and biological processes in the ocean. Considering rapid warming and associated sea ice melt in the Arctic is leading to changing carbon dynamics, we should require even more of this tracer data. To date however, there exists only a handful of studies in this region (e.g. Griffith et al., 2012; Druffel et al., 2017). This is likely, in large part, due to a persistent, variable sea ice cover in the region making it a difficult environment to navigate (Shen et al., 2021). Even so, we present testable hypotheses in this thesis and urge the scientific community to continue researching Arctic carbon cycling through DIC concentrations and isotopes. For starters, we suggest sampling for DIC $\delta^{13}C$ and $\Delta^{14}C$ following the transect taken by Lehmann and coworkers (2022) through Parry Channel between M'Clure Strait and Lancaster Sound. Additionally, we urge the radiocarbon community to agree upon and routinely sample one historical station in the Beaufort Sea, such that we may quantify and document changes to the depth of penetration and rates of sequestration of C_{anth} in different Canadian Arctic water masses (as per the Suess effect). We should not take a wait-and-see approach to the current climate crisis, but rather go out and document what is happening now. If we cannot fix it, then we will still be better off having the knowledge to prepare for the future. This thesis provides the most comprehensive CAA DIC isotope dataset to date and seeks to fuel discussions around real, measured large-scale carbon cycling in this globally important environment. We make this data freely available to the scientific community and support continued work in these Canadian Arctic regions.

10. References

Aagaard, K., Coachman, L. K., & Carmack, E. (1981). On the halocline of the Arctic Ocean. *Deep Sea Research Part A. Oceanographic Research Papers*, *28*(6), 529-545. doi: 10.1016/0198-0149(81)90115-1

Aagaard, K., & Carmack, E. C. (1989). The role of sea ice and other fresh water in the Arctic circulation. *Journal of Geophysical Research: Oceans*, *94*(C10), 14485-14498. doi: 10.1029/JC094iC10p14485

Aagaard, K., & Carmack, E. C. (1994). The Arctic Ocean and climate: A perspective. *Washington DC American Geophysical Union Geophysical Monograph Series*, *85*, 5-20. doi: 10.1029/GM085p0005

Afsharipour, Y., Xu, C., Myers, P. G., Else, B., & Zhou, Q. (2023). Numerical Investigation of Diapycnal Mixing of the Kitikmeot Sea in the Southern Canadian Arctic Archipelago. *Atmosphere-Ocean*, 1-16. doi: 10.1080/07055900.2023.2294210

Alkire, M. B., Jacobson, A. D., Lehn, G. O., Macdonald, R. W., & Rossi, M. W. (2017). On the geochemical heterogeneity of rivers draining into the straits and channels of the Canadian Arctic Archipelago. *Journal of Geophysical Research: Biogeosciences*, *122*(10), 2527-2547. doi: 10.1002/2016JG003723.

Alling, V., Porcelli, D., Mörth, C. M., Anderson, L. G., Sanchez-Garcia, L., Gustafsson, Ö., Andersson, P.S., & Humborg, C. (2012). Degradation of terrestrial organic carbon, primary production and out-gassing of CO2 in the Laptev and East Siberian Seas as inferred from δ13C values of DIC. *Geochimica et Cosmochimica Acta*, *95*, 143-159. doi: 10.1016/j.gca.2012.07.028

Ardyna, M., & Arrigo, K. R. (2020). Phytoplankton dynamics in a changing Arctic Ocean. *Nature Climate Change*, *10*(10), 892-903. doi: 10.1038/s41558-020-0905-y

Azetsu-Scott, K., Clarke, A., Falkner, K., Hamilton, J., Jones, E. P., Lee, C., ... & Yeats, P. (2010). Calcium carbonate saturation states in the waters of the Canadian Arctic Archipelago and the Labrador Sea. *Journal of Geophysical Research: Oceans*, *115*(C11). doi: 10.1029/2009JC005917

Azetsu-Scott, K., Petrie, B., Yeats, P., and Lee, C. (2012). Composition and Fluxes of Freshwater Through Davis Strait Using Multiple Chemical Tracers. J. Geophys. Res. Oceans. 117, C12011. doi: 10.1029/2012JC008172

Back, D. Y., Ha, S. Y., Else, B., Hanson, M., Jones, S. F., Shin, K. H., ... & Mundy, C. J. (2021). On the impact of wastewater effluent on phytoplankton in the Arctic coastal zone: a case study in the Kitikmeot Sea of the Canadian Arctic. *Science of the Total Environment*, *764*, 143861. doi: 10.1016/j.scitotenv.2020.143861

Bauch, D., Polyak, L., & Ortiz, J. D. (2015). A baseline for the vertical distribution of the stable carbon isotopes of dissolved inorganic carbon (δ13C DIC) in the Arctic Ocean. *Arktos*, *1*, 1-13. doi: 10.1007/s41063-015-0001-0

Beaupré-Laperrière, A., Mucci, A., & Thomas, H. (2020). The recent state and variability of the carbonate system of the Canadian Arctic Archipelago and adjacent basins in the context of ocean acidification. *Biogeosciences*, *17*(14), 3923-3942. doi: 10.5194/bg-17-3923-2020

Broecker, W. S., Peng, T. H., Ostlund, G., & Stuiver, M. (1985). The distribution of bomb radiocarbon in the ocean. *Journal of Geophysical Research: Oceans*, *90*(C4), 6953-6970. doi: 10.1029/JC090iC04p06953

Brown, K. A., Miller, L. A., Mundy, C. J., Papakyriakou, T., Francois, R., Gosselin, M., … & Tortell, P. D. (2015). Inorganic carbon system dynamics in landfast Arctic sea ice during the early-melt period. *Journal of Geophysical Research: Oceans*, *120*(5), 3542-3566. doi: 10.1002/2014JC010620

Brown, K. A., Williams, W., Carmack, E., Schimnowski, A., Nivingalok, J., and Clarke, C. 2016. Where the river meets the sea: Investigating nutrient dynamics in the Kitikmeot riverine-coastal domain. ArcticNet Annual Scientific Meeting, Winnipeg, Man., December 2016. [poster presentation].

Brown, K. A., Williams, W. J., Carmack, E. C., Fiske, G., François, R., McLennan, D., & Peucker-Ehrenbrink, B. (2020). Geochemistry of small Canadian Arctic Rivers with diverse geological and hydrological settings. *Journal of Geophysical Research: Biogeosciences*, *125*(1), e2019JG005414. doi: 10.1029/2019JG005414

Campeau, A., Soerensen, A. L., Martma, T., Åkerblom, S., & Zdanowicz, C. (2020). Controls on the 14C content of dissolved and particulate organic carbon mobilized across the Mackenzie River Basin, Canada. *Global Biogeochemical Cycles*, *34*(12), e2020GB006671. doi: 10.1029/2020GB006671

Codispoti, L. A., Flagg, C., Kelly, V., & Swift, J. H. (2005). Hydrographic conditions during the 2002 SBI process experiments. *Deep Sea Research Part II: Topical Studies in Oceanography*, *52*(24-26), 3199-3226. doi: 10.1016/j.dsr2.2005.10.007

Curry, B., Lee, C. M., & Petrie, B. (2011). Volume, freshwater, and heat fluxes through Davis Strait, 2004–05. *Journal of Physical Oceanography*, *41*(3), 429-436. doi: 10.1175/2010JPO4536.1

DeGrandpre, M., Evans, W., Timmermans, M. L., Krishfield, R., Williams, B., & Steele, M. (2020). Changes in the Arctic Ocean carbon cycle with diminishing ice cover. *Geophysical Research Letters*, *47*(12), e2020GL088051. doi: 10.1029/2020GL088051

Druffel, E. R. M., Griffin, S., Glynn, C. S., Benner, R., & Walker, B. D. (2017). Radiocarbon in dissolved organic and inorganic carbon of the Arctic Ocean. *Geophysical Research Letters*, *44*(5), 2369-2376. doi: 10.1002/2016GL072138

Else, B. G., Galley, R. J., Lansard, B., Barber, D. G., Brown, K., Miller, L. A., ... & Rysgaard, S. (2013). Further observations of a decreasing atmospheric CO2 uptake capacity in the Canada Basin (Arctic Ocean) due to sea ice loss. *Geophysical Research Letters*, *40*(6), 1132-1137. doi: 10.1002/grl.50268

Emerson, S., & Hedges, J. (2008). *Chemical oceanography and the marine carbon cycle*. Cambridge University Press.

England, M. R., Eisenman, I., Lutsko, N. J., & Wagner, T. J. (2021). The recent emergence of Arctic Amplification. *Geophysical Research Letters*, *48*(15), e2021GL094086. doi: 10.1029/2021GL094086

Fox, A., & Walker, B. D. (2022). Sources and Cycling of Particulate Organic Matter in Baffin Bay: A Multi-Isotope δ13C, δ15N, and Δ14C Approach. *Frontiers in Marine Science*, *9*, 846025. doi: 10.3389/fmars.2022.846025

Gao, P., Xu, X., Zhou, L., Pack, M. A., Griffin, S., Santos, G. M., … & Liu, K. (2014). Rapid sample preparation of dissolved inorganic carbon in natural waters using a headspace-extraction approach for radiocarbon analysis by accelerator mass spectrometry. *Limnology and Oceanography: Methods*, *12*(4), 174-190. doi: 10.4319/lom.2014.12.174

Granger, J., Sigman, D. M., Gagnon, J., Tremblay, J. É., & Mucci, A. (2018). On the properties of the Arctic halocline and deep water masses of the Canada Basin from nitrate isotope ratios. *Journal of Geophysical Research: Oceans*, *123*(8), 5443-5458. doi: 10.1029/2018JC014110

Griffith, D. R., McNichol, A. P., Xu, L., McLaughlin, F. A., Macdonald, R. W., Brown, K. A., & Eglinton, T. I. (2012). Carbon dynamics in the western Arctic Ocean: insights from full-depth carbon isotope profiles of DIC, DOC, and POC. *Biogeosciences*, *9*(3), 1217-1224. doi: 10.5194/bg-9-1217-2012

Guilderson, T. P., Caldeira, K., & Duffy, P. B. (2000). Radiocarbon as a diagnostic tracer in ocean and carbon cycle modeling. *Global Biogeochemical Cycles*, *14*(3), 887-902. doi: 10.1029/1999GB001192

Holland, M. M., & Bitz, C. M. (2003). Polar amplification of climate change in coupled models. Climate dynamics, 21(3-4), 221-232. doi: 10.1007/s00382-003-0332-6

Ingram, R. G., & Prinsenberg, S. (1998). Coastal oceanography of Hudson Bay and surrounding eastern Canadian Arctic waters. *The sea*, *11*(29), 835-859.

IPCC, 2023: *Climate Change 2023: Synthesis Report. Contribution of Working Groups I, II and III to the Sixth Assessment Report of the Intergovernmental Panel on Climate Change* [Core Writing Team, H. Lee and J. Romero (eds.)]. IPCC, Geneva, Switzerland, 184 pp. doi: 10.59327/IPCC/AR6-9789291691647.

Jakobsson, M. (2002). Hypsometry and volume of the Arctic Ocean and its constituent seas. *Geochemistry, Geophysics, Geosystems*, *3*(5), 1-18. doi: 10.1029/2001GC000302

Johnson, K. M., Wills, K. D., Butler, D. B., Johnson, W. K., & Wong, C. S. (1993). Coulometric total carbon dioxide analysis for marine studies: maximizing the performance of an automated gas extraction system and coulometric detector. *Marine Chemistry*, *44*(2-4), 167-187. doi: 10.1016/0304-4203(93)90201-X

Jones, E. P., Swift, J. H., Anderson, L. G., Lipizer, M., Civitarese, G., Falkner, K. K., Kattner, G., & McLaughlin, F. (2003). Tracing Pacific water in the North Atlantic Ocean. *Journal of Geophysical Research: Oceans*, *108*(C4). doi: 10.1029/2001JC001141

Keeling, C. D. (1979). The Suess effect: 13Carbon-14Carbon interrelations. *Environment International*, *2*(4-6), 229-300. doi: 10.1016/0160-4120(79)90005-9

Koeve, W., Wagner, H., Kähler, P., & Oschlies, A. (2015). 14 C-age tracers in global ocean circulation models. *Geoscientific Model Development*, *8*(7), 2079-2094. doi: 10.5194/gmd-8-2079-2015

Körtzinger, A., Quay, P. D., & Sonnerup, R. E. (2003). Relationship between anthropogenic CO2 and the 13C Suess effect in the North Atlantic Ocean. *Global Biogeochemical Cycles*, *17*(1), 5-1. doi: 10.1029/2001GB001427

Kroopnick, P. M. (1985). The distribution of 13C of ΣCO2 in the world oceans. *Deep Sea Research Part A. Oceanographic Research Papers*, *32*(1), 57-84. doi: 10.1016/0198-0149(85)90017-2

Landschützer, P., Gruber, N., & Bakker, D. C. (2016). Decadal variations and trends of the global ocean carbon sink. *Global Biogeochemical Cycles*, *30*(10), 1396-1417. doi: 10.1002/2015GB005359

Lavoie, D., Denman, K., & Michel, C. (2005). Modeling ice algal growth and decline in a seasonally ice-covered region of the Arctic (Resolute Passage, Canadian Archipelago). *Journal of Geophysical Research: Oceans*, *110*(C11). doi: 10.1029/2005JC002922

Lehmann, N., Kienast, M., Granger, J., & Tremblay, J. É. (2022). Physical and biogeochemical influences on nutrients through the Canadian Arctic Archipelago: Insights from nitrate isotope ratios. *Journal of Geophysical Research: Oceans*, *127*(3), e2021JC018179. doi: 10.1029/2021JC018179

Letscher, R. T., Hansell, D. A., & Kadko, D. (2011). Rapid removal of terrigenous dissolved organic carbon over the Eurasian shelves of the Arctic Ocean. *Marine Chemistry*, *123*(1-4), 78-87. doi: 10.1016/j.marchem.2010.10.002

MacGilchrist, G. A., Garabato, A. N., Tsubouchi, T., Bacon, S., Torres-Valdés, S., & Azetsu-Scott, K. (2014). The arctic ocean carbon sink. *Deep Sea Research Part I: Oceanographic Research Papers*, *86*, 39-55. doi: 10.1016/j.dsr.2014.01.002

Mahadevan, A. (2001). An analysis of bomb radiocarbon trends in the Pacific. *Marine Chemistry*, *73*(3-4), 273-290. doi: 10.1016/S0304-4203(00)00113-4

Mathis, J. T., Pickart, R. S., Byrne, R. H., McNeil, C. L., Moore, G. W. K., Juranek, L. W., … & Feely, R. A. (2012). Storm-induced upwelling of high pCO2 waters onto the continental shelf of the western Arctic Ocean and implications for carbonate mineral saturation states. *Geophysical Research Letters*, *39*(7). doi: 10.1029/2012GL051574

McGuire, A. D., Anderson, L. G., Christensen, T. R., Dallimore, S., Guo, L., Hayes, D. J., … & Roulet, N. (2009). Sensitivity of the carbon cycle in the Arctic to climate change. *Ecological Monographs*, *79*(4), 523-555. doi: 10.1890/08-2025.1

McLaughlin, F. A., Carmack, E. C., Ingram, R. G., Williams, W. J., & Michel, C. (2005). Oceanography of the Northwest Passage (26, P). *The sea*, *14*.

Miller, L. A., Macdonald, R. W., McLaughlin, F., Mucci, A., Yamamoto-Kawai, M., Giesbrecht, K. E., & Williams, W. J. (2014). Changes in the marine carbonate system of the western Arctic: patterns in a rescued data set. *Polar Research*, *33*(1), 20577. doi: 10.3402/polar.v33.20577

Mol, J., Thomas, H., Myers, P. G., Hu, X., & Mucci, A. (2018). Inorganic carbon fluxes on the Mackenzie Shelf of the Beaufort Sea. *Biogeosciences*, *15*(4), 1011-1027. doi: 10.5194/bg-15-1011-2018

Mook, W. G., Bommerson, J. C., & Staverman, W. H. (1974). Carbon isotope fractionation between dissolved bicarbonate and gaseous carbon dioxide. *Earth and planetary science letters*, *22*(2), 169-176. doi: 10.1016/0012-821X(74)90078-8

Mucci, A., Lansard, B., Miller, L. A., & Papakyriakou, T. N. (2010). CO2 fluxes across the air-sea interface in the southeastern Beaufort Sea: Ice-free period. *Journal of Geophysical Research: Oceans*, *115*(C4). doi: 10.1029/2009JC005330

Münchow, A., Falkner, K. K., & Melling, H. (2015). Baffin island and west Greenland current systems in northern Baffin bay. *Progress in Oceanography*, *132*, 305-317. doi: 10.1016/j.pocean.2014.04.001

Olack, G. A., Colman, A. S., Pfister, C. A., & Wootton, J. T. (2018). Seawater DIC analysis: The effects of blanks and long-term storage on measurements of concentration and stable isotope composition. *Limnology and Oceanography: Methods*, *16*(3), 160-179. doi: 10.1002/lom3.10235

Olsen, A., Anderson, L. G., & Heinze, C. (2015). Arctic carbon cycle: Patterns, impacts and possible changes. *The New Arctic*, 95-115. doi: 10.1007/978-3-319-17602-4_8

Östlund, H. G., Top, Z., & Lee, V. E. (1982). Isotope dating of waters at Fram III. *Geophysical Research Letters*, *9*(9), 1117-1119. doi: 10.1029/GL009i009p01117

Östlund, H. G., Possnert, G., & Swift, J. H. (1987). Ventilation rate of the deep Arctic Ocean from carbon 14 data. *Journal of Geophysical Research: Oceans*, *92*(C4), 3769-3777. doi: 10.1029/JC092iC04p03769
Ouyang, Z., Qi, D., Chen, L., Takahashi, T., Zhong, W., DeGrandpre, M. D., ... & Cai, W. J. (2020). Sea-ice loss amplifies summertime decadal CO2 increase in the western Arctic Ocean. *Nature Climate Change*, *10*(7), 678-684. doi: 10.1038/s41558-020-0784-2

Papakyriakou, T., & Miller, L. (2011). Springtime CO2 exchange over seasonal sea ice in the Canadian Arctic Archipelago. *Annals of Glaciology*, *52*(57), 215-224. doi: 10.3189/172756411795931534

Park, H. S., Kim, S. J., Stewart, A. L., Son, S. W., & Seo, K. H. (2019). Mid-holocene Northern Hemisphere warming driven by Arctic amplification. *Science advances*, *5*(12), eaax8203. doi: 10.1126/sciadv.aax8203

Rantanen, M., Karpechko, A. Y., Lipponen, A., Nordling, K., Hyvärinen, O., Ruosteenoja, K., … & Laaksonen, A. (2022). The Arctic has warmed nearly four times faster than the globe since 1979. *Communications Earth & Environment*, *3*(1), 168. doi: 10.1038/s43247-022-00498-3

Reimer, P. J., Brown, T. A., & Reimer, R. W. (2004). Discussion: reporting and calibration of post-bomb 14C data. *Radiocarbon*, *46*(3), 1299-1304. doi: 10.1017/S0033822200033154

Revelle, R., & Suess, H. E. (1957). Carbon dioxide exchange between atmosphere and ocean and the question of an increase of atmospheric CO2 during the past decades. *Tellus*, *9*(1), 18-27. doi: 10.3402/tellusa.v9i1.9075

Sakshaug, E. (2004). Primary and secondary production in the Arctic Seas. In *The organic carbon cycle in the Arctic Ocean* (pp. 57-81). Berlin, Heidelberg: Springer Berlin Heidelberg. doi: 10.1007/978-3-642-18912-8_3

Sarmiento, J. L. (2006). *Ocean biogeochemical dynamics*. Princeton university press. doi: 10.1515/9781400849079

Serreze, M. C., & Francis, J. A. (2006). The Arctic amplification debate. *Climatic change*, *76*(3-4), 241-264. doi: 10.1007/s10584-005-9017-y

Shadwick, E. H., Thomas, H., Chierici, M., Else, B., Fransson, A., Michel, C., ... & Tremblay, J. É. (2011). Seasonal variability of the inorganic carbon system in the Amundsen Gulf region of

the southeastern Beaufort Sea. *Limnology and Oceanography*, *56*(1), 303-322. doi: 10.4319/lo.2011.56.1.0303

Shen, X. Y., Zhang, Y., Chen, C. S., Hu, S., Xu, D. Y., Shao, W. Z., ... & Feng, G. P. (2021). Arctic sea ice variation in the Northwest Passage in 1979–2017 and its response to surface thermodynamics factors. *Advances in Climate Change Research*, *12*(4), 563-580. doi: 10.1016/j.accre.2021.08.004

Stuiver, M., & Polach, H. A. (1977). Discussion reporting of 14C data. *Radiocarbon*, *19*(3), 355-363. doi: 10.1017/S0033822200003672

Tamše, S., Ogrinc, N., Walter, L. M., Turk, D., & Faganeli, J. (2015). River sources of dissolved inorganic carbon in the gulf of Trieste (N Adriatic): stable carbon isotope evidence. *Estuaries and Coasts*, *38*, 151-164. doi: 10.1007/s12237-014-9812-7

Tao, R., & Myers, P. G. (2022). Modelling the Oceanic Advection of Pollutants Spilt Along with the Northwest Passage. *Atmosphere-Ocean*, *60*(2), 88-101. doi: 10.1080/07055900.2022.2065965

Timmermans, M. L., & Garrett, C. (2006). Evolution of the deep water in the Canadian Basin in the Arctic Ocean. *Journal of physical oceanography*, *36*(5), 866-874. doi: 10.1175/JPO2906.1

Torres, M. E., Mix, A. C., & Rugh, W. D. (2005). Precise δ13C analysis of dissolved inorganic carbon in natural waters using automated headspace sampling and continuous-flow mass spectrometry. *Limnology and Oceanography: Methods*, *3*(8), 349-360. doi: 10.4319/lom.2005.3.349

Tremblay, J. É., Simpson, K., Martin, J., Miller, L., Gratton, Y., Barber, D., & Price, N. M. (2008). Vertical stability and the annual dynamics of nutrients and chlorophyll fluorescence in the coastal, southeast Beaufort Sea. *Journal of Geophysical Research: Oceans*, *113*(C7). doi: 10.1029/2007JC004547

Tremblay, J. É., Anderson, L. G., Matrai, P., Coupel, P., Bélanger, S., Michel, C., & Reigstad, M. (2015). Global and regional drivers of nutrient supply, primary production and CO2 drawdown in the changing Arctic Ocean. *Progress in Oceanography*, *139*, 171-196. doi: 10.1016/j.pocean.2015.08.009

Vargas, C. A., Cantarero, S. I., Sepúlveda, J., Galán, A., De Pol-Holz, R., Walker, B., ... & Salisbury, J. (2021). A source of isotopically light organic carbon in a low-pH anoxic marine zone. *Nature communications*, *12*(1), 1604. doi: 10.1038/s41467-021-21871-4

Varela, D. E., Crawford, D. W., Wrohan, I. A., Wyatt, S. N., & Carmack, E. C. (2013). Pelagic primary productivity and upper ocean nutrient dynamics across Subarctic and Arctic Seas. *Journal of Geophysical Research: Oceans*, *118*(12), 7132-7152. doi: 10.1002/2013JC009211

Walker, B. D., & Xu, X. (2019). An improved method for the sealed-tube zinc graphitization of microgram carbon samples and 14C AMS measurement. *Nuclear Instruments and Methods in Physics Research Section B: Beam Interactions with Materials and Atoms*, *438*, 58-65. doi: 10.1016/j.nimb.2018.08.004

Watanabe, E. (2011). Beaufort shelf break eddies and shelf-basin exchange of Pacific summer water in the western Arctic Ocean detected by satellite and modeling analyses. *Journal of Geophysical Research: Oceans*, *116*(C8). doi: 10.1029/2010JC006259

Williams, W., Brown, K. A., Bluhm, B., Carmack, E. C., Dalman, L., Danielson, S. L., ... & Schimnowski, A. (2018). Stratification in the Canadian Arctic Archipelago's Kitikmeot Sea: biological and geochemical consequences. *Polar Knowledge: Aqhaliat Report*, *1*(1), 46-52. doi: 10.35298/pkc.2018.06

Xu, X., Trumbore, S. E., Zheng, S., Southon, J. R., McDuffee, K. E., Luttgen, M., & Liu, J. C. (2007). Modifying a sealed tube zinc reduction method for preparation of AMS graphite targets: Reducing background and attaining high precision. *Nuclear Instruments and Methods in Physics Research Section B: Beam Interactions with Materials and Atoms*, *259*(1), 320-329. doi: 10.1016/j.nimb.2007.01.175

Xu, C., Mikhael, W., Myers, P. G., Else, B., Sims, R. P., & Zhou, Q. (2021). Effects of seasonal ice coverage on the physical oceanographic conditions of the Kitikmeot Sea in the Canadian Arctic Archipelago. *Atmosphere-Ocean*, *59*(4-5), 214-232. doi: 10.1080/07055900.2021.1965531

Yamamoto-Kawai, M., McLaughlin, F. A., Carmack, E. C., Nishino, S., & Shimada, K. (2008). Freshwater budget of the Canada Basin, Arctic Ocean, from salinity, δ18O, and nutrients. *Journal of Geophysical Research: Oceans*, *113*(C1). doi: 10.1029/2006JC003858

Zeidan, S., Walker, J., Else, B. G., Miller, L. A., Azetsu-Scott, K., & Walker, B. D. (2022). Using Radiocarbon Measurements of Dissolved Inorganic Carbon to Determine a Revised Residence Time for Deep Baffin Bay. *Frontiers in Marine Science*, *9*, 845536. doi: 10.3389/fmars.2022.845536

Zhang, J., Quay, P. D., & Wilbur, D. O. (1995). Carbon isotope fractionation during gas-water exchange and dissolution of CO2. *Geochimica et Cosmochimica Acta*, *59*(1), 107-114. doi: 10.1016/0016-7037(95)91550-D

Appendix A: Supplementary Figure

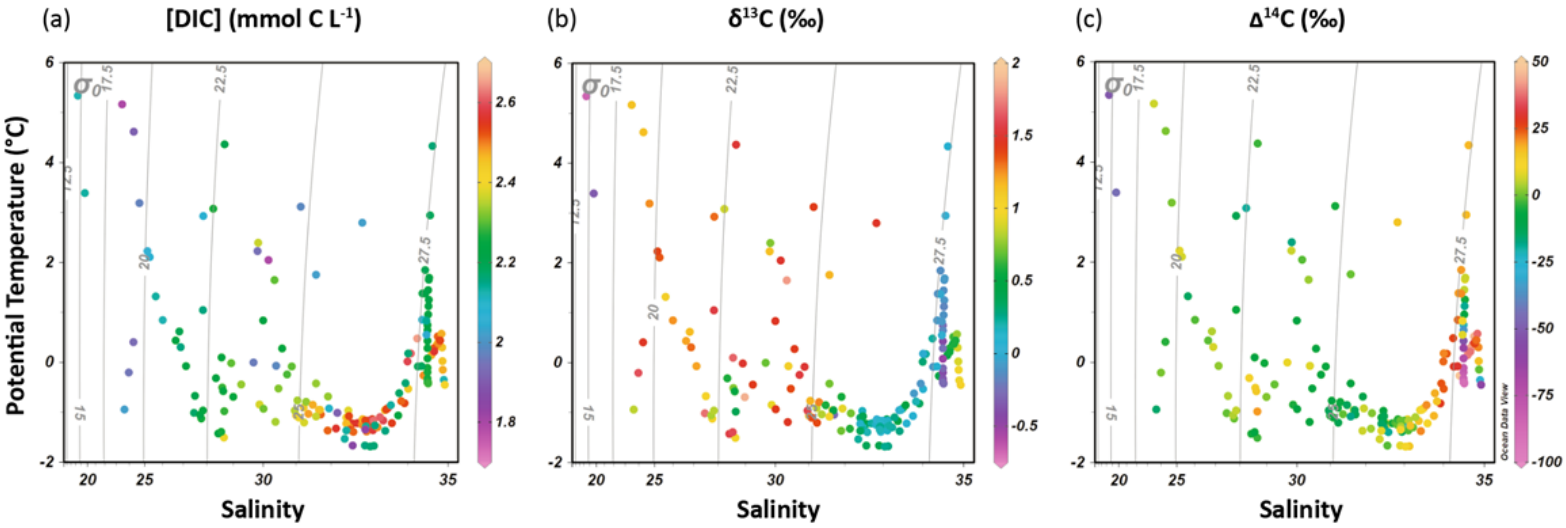

Figure S1. Potential temperature-salinity plots with measured DIC parameters. (a) potential temperature and salinity with [DIC] colour bar, (b) potential temperature and salinity with $\delta^{13}C$ colour bar, (c) potential temperature and salinity with age-corrected DIC $\Delta^{14}C$ colour bar. Solid grey lines show potential density anomaly contours measured as σ_θ in kg m^{-3}. For water mass endmembers, please refer to Figure 3.

Appendix B: Supplementary and Extended Tables

Table S1. Sampling information for stations occupied by the CCGS Amundsen during the 2019 Baffin Bay cruise (Cruise# 1902; Zeidan et al., 2022) and the Canadian Arctic Archipelago during the 2021 RadCARBBS (Cruise# 2104) expedition.

Cruise	Station	Latitude (°N)	Longitude (°W)	Date	Bottom Depth (m)
RadCARBBS	C002	73.958	-88.824	21/09/11	419
	C003	72.366	-91.406	21/09/11	388
	C004	71.956	-95.839	21/09/11	425
	C009	70.708	-98.965	21/09/12	2001
	312	69.170	-100.700	21/09/13	68
	C010	68.249	-101.643	21/09/13	105
	C011	69.018	-106.609	21/09/15	113
	C012	68.329	-110.268	21/09/15	292
	C013	69.056	-114.786	21/09/16	91
	C014	69.617	-118.605	21/09/16	517
	405	70.665	-122.621	21/09/17	586
	414	71.495	-127.136	21/09/19	304
	PCB07	70.420	-131.540	21/09/22	51
	434	70.178	-133.554	21/09/23	45
	476	69.998	-138.629	21/09/28	270
	PCB12	70.277	-135.775	21/09/30	54
	546	71.743	-133.946	21/10/01	1607
	515	75.103	-120.628	21/10/04	488
	518	74.598	-121.451	21/10/04	435
[1]Baffin Bay	193	66.770	-59.340	19/07/09	957
	196	66.987	-56.059	19/07/10	130
	BB15	68.451	-55.900	19/07/11	492
	BB18	70.090	-52.740	19/07/12	498
	227	70.797	-56.988	19/07/13	536
	224	70.420	-62.945	19/07/15	2092
	BB2	72.749	-66.995	19/07/17	2367
	204	73.269	-57.999	19/07/18	959
	210	75.419	-61.560	19/07/19	1171
	108	76.258	-74.599	19/07/22	443
	323	74.160	-80.471	19/07/24	789

[1]Zeidan et al., 2022

Table S2. Summary of measured physical data and dissolved inorganic carbon (DIC) values generated from sampling stations occupied by the CCGS Amundsen during the 2019 Baffin Bay (Cruise# 1902; Zeidan et al., 2022) and 2021 RadCARBBS (Cruise# 2104) expeditions. Depth (pressure; Dbars), temperature and salinity were measured using a SBE 911plus CTD attached to the sampling rosette. DIC $\delta^{13}C$ values were measured at the Ján Veizer Stable Isotope Laboratory at the University of Ottawa for both this paper and by Zedian and coworkers (2022). DIC $\Delta^{14}C$, fraction modern and ^{14}C ages were measured at the University of Ottawa A.E.L AMS Laboratory for RadCARBBS samples and at the Keck Carbon Cycle AMS facility at the University of California, Irvine, for the Baffin Bay dataset.

Station	Cruise	Temp	Salinity	Veizer Lab ID	$\delta^{13}C$	Error	[DIC]	Error	AMS #	Fraction Modern	Error	$\Delta^{14}C$	Error	^{14}C Age	Error
(Dbars)	(cast #)	(°C)			(‰)	(±)	(mmol/L C)	(±)			(±)	(‰)	(±)	(BP)	(±)
C002	***RadCARBBS***														
404	2	0.5	34.23	C-157056	0.21	0.05	2.65		UOC-19475	1.0347	0.0016	25.9	1.6	-270	15
298	2	0.0	33.99	C-157057	0.29	0.08	2.59		UOC-19474	1.0317	0.0016	22.9	1.6	-245	15
198	2	-1.2	33.37	C-157058	0.45	0.06	2.59		UOC-19473	1.0246	0.0016	15.9	1.6	-190	15
149	2	-1.2	32.57	C-157059	0.37	0.05	2.55	0.00	UOC-19472	1.0133	0.0016	4.6	1.6	-100	15
				C-157060	0.39	0.08	2.56		UOC-19468	1.0155	0.0016	6.8	1.6	-120	15
				C-157061	0.39	0.06	2.55								
100	2	-1.3	32.13	C-157062	0.59	0.04	2.56		UOC-19467	1.0116	0.0016	2.9	1.6	-85	15
50	2	-1.0	31.36	C-157063	0.81	0.05	2.48		UOC-19466	1.0076	0.0015	-1.0	1.5	-55	15
20	2	-0.7	28.98	C-157064	1.86	0.07	2.25		UOC-19465	1.0097	0.0016	1.0	1.6	-70	15
2	2	-1.0	27.46	C-157065	1.70	0.04	2.17		UOC-19464	1.0079	0.0017	-0.8	1.7	-60	15
C003	***RadCARBBS***														
297	3	0.2	34.07	C-157033	0.22	0.08	2.61		UOC-19487	1.0329	0.0017	24.0	1.7	-255	15
178	3	-0.9	33.49	C-157034	0.33	0.06	2.59		UOC-19486	1.0256	0.0016	16.9	1.6	-200	15
									UOC-20615	1.0236	0.0016	14.8	1.6	-180	15
144	3	-1.1	33.09	C-157035	0.34	0.05	2.54		UOC-19485	1.0208	0.0017	12.0	1.7	-160	15
99	3	-1.3	32.51	C-157036	0.38	0.04	2.54		UOC-19482	1.0175	0.0016	8.8	1.6	-135	15
50	3	-1.4	31.90	C-157038	0.69	0.05	2.51	0.00	UOC-19480	1.0126	0.0016	3.9	1.6	-95	15
				C-157039	0.69	0.04	2.51		UOC-19478	1.0113	0.0016	7.7	1.6	-85	15
				C-157040	0.72	0.04	2.52								
30	3	-1.0	31.66	C-157037	1.08	0.04	2.46		UOC-19481	1.0130	0.0016	4.3	1.6	-100	15

4	3	1.6	30.35	C-157041	1.80	0.05	2.30		UOC-19479	1.0164	0.0016	2.6	1.6	-125	15
C004	***RadCARBBS***														
411	4	-1.2	33.00	C-157023	0.04	0.05	2.59		UOC-19656	1.0071	0.0014	-1.5	1.4	-50	15
297	4	-1.2	32.94	C-157024	0.19	0.06	2.57		UOC-19655	1.0078	0.0014	-0.8	1.4	-55	15
				C-157026	0.16	0.09	2.59	0.00							
				C-157025	0.09	0.08	2.57		UOC-19654	1.0085	0.0014	-0.2	1.4	-65	15
178	4	-1.2	32.77	C-157027	0.21	0.08	2.56		UOC-19653	1.0061	0.0014	-2.5	1.4	-45	15
									UOC-20616	1.0062	0.0015	-2.4	1.5	-45	15
139	4	-1.2	32.70	C-157028	0.22	0.06	2.56		UOC-19649	1.0018	0.0014	-6.8	1.4	-10	15
99	4	-1.2	32.48	C-157029	0.43	0.09	2.56		UOC-19648	1.0013	0.0014	-7.3	1.4	-5	15
50	4	-0.9	31.22	C-157030	0.84	0.09	2.44		UOC-19647	0.9995	0.0014	-9.1	1.4	5	15
20	4	0.0	28.91	C-157031	1.49	0.08	2.30		UOC-19646	1.0025	0.0015	-6.0	1.5	-15	15
2	4	0.4	24.28	C-157032	1.46	0.10	1.93		UOC-19645	1.0043	0.0015	-4.3	1.5	-30	15
C009	***RadCARBBS***														
178	6	-1.1	33.29	C-156682	0.26	0.06	2.61		UOC-19495	1.0204	0.0016			-155	15
									UOC-20617	1.0126	0.0015	3.9	1.5	-95	15
139	6	-1.2	33.12	C-156683	0.14	0.04	2.62		UOC-19494	1.0127	0.0016	4.0	1.6	-95	15
99	6	-1.2	32.84	C-156684	0.15	0.06	2.59		UOC-19493	1.0121	0.0017	3.4	1.7	-90	15
38	6	-1.1	31.00	C-156685	1.13	0.05	2.41		UOC-19492	1.0034	0.0016	-5.1	1.6	-25	15
20	6	-0.4	29.26	C-156686	1.43	0.06	2.34	0.02	UOC-19491	1.0088	0.0017	0.2	1.7	-65	15
				C-156687	1.43	0.07	2.31		UOC-19489	1.0071	0.0016	-1.5	1.6	-50	15
3	6	-0.2	23.97	C-156688	1.62	0.06	1.95		UOC-19488	1.0091	0.0018	0.5	1.8	-70	15
312	***RadCARBBS***														
50	7	-0.8	29.87	C-156677	0.93	0.08	2.37		UOC-19841	1.0038	0.0016	-4.8	1.6	-25	15
14	7	0.4	26.64	C-156678	1.21	0.11	2.22		UOC-19840	1.0074	0.0017	-1.3	1.7	-55	15
2	7	0.9	26.00	C-156680	1.20	0.08	2.11	0.01	UOC-19838	1.0078	0.0017	-0.9	1.7	-55	15
				C-156681	1.20	0.09	2.13								
				C-156679	1.33	0.09	2.12		UOC-19839	1.0060	0.0017	-2.6	1.7	-45	15
C010	***RadCARBBS***														
90	8	-1.5	28.65	C-156671	0.96	0.07	2.39		UOC-19849	1.0055	0.0016	-3.1	1.6	-40	15
36	8	-1.1	27.77	C-156673	1.05	0.06	2.26		UOC-19848	1.0082	0.0016	-0.4	1.6	-60	15

				C-156674	1.02	0.09	2.26	0.01							
				C-156672	1.03	0.07	2.27		UOC-19847	1.0081	0.0016	-0.5	1.6	-60	15
20	8	-0.1	27.11	C-156675	1.21	0.07	2.22		UOC-19846	1.0106	0.0017	1.9	1.7	-80	15
3	8	2.1	25.29	C-156676	1.35	0.10	2.07		UOC-19842	1.0151	0.0017	6.5	1.7	-115	15
C011	***RadCARBBS***														
99	12	-1.0	27.72	C-156652	0.80	0.06	2.22	0.03	UOC-19855	1.0128	0.0016	4.2	1.6	-95	15
				C-156653	0.79	0.06	2.18		UOC-19856	1.0120	0.0017	3.4	1.7	-90	15
				C-156654	0.82	0.06	2.22								
49	12	-0.7	27.51	C-156655	1.03	0.06	2.20		UOC-19854	1.0123	0.0016	3.7	1.6	-95	15
30	12	0.6	26.81	C-156656	1.15	0.06	2.19		UOC-19853	1.0126	0.0017	4.0	1.7	-95	15
2	12	3.2	24.68	C-156657	1.25	0.05	1.97		UOC-19852	1.0090	0.0017	0.4	1.7	-65	15
C012	***RadCARBBS***														
282	13	-1.0	28.66	C-156644	0.37	0.06	2.28		UOC-20205	1.0285	0.0015	19.7	1.5	-220	15
178	13	-0.6	28.62	C-156646	0.42	0.06	2.24	0.00	UOC-20203	1.0257	0.0015	17.0	1.5	-200	15
				C-156645	0.61	0.06	2.23		UOC-20614	1.0216	0.0016	12.8	1.6	-165	15
139	13	-0.5	28.58	C-156647	0.73	0.07	2.28		UOC-20199	1.0230	0.0015	14.2	1.5	-175	15
99	13	-0.3	28.35	C-156648	0.58	0.05	2.22		UOC-20198	1.0217	0.0015	13.0	1.5	-170	15
50	13	-1.0	27.84	C-156649	0.82	0.06	2.24		UOC-20197	1.0138	0.0015	5.1	1.5	-105	15
23	13	0.3	26.87	C-156650	1.31	0.06	2.15		UOC-20196	1.0153	0.0015	6.6	1.5	-115	15
5	13	2.2	25.16	C-156651	1.39	0.05	2.06		UOC-20195	1.0165	0.0014	7.8	1.4	-125	15
C013	***RadCARBBS***														
82	15	-1.0	32.46	C-156306	0.16	0.07	2.38		UOC-19662	0.9994	0.0014	-9.2	1.4	5	15
40	15	-0.4	31.58	C-156307	0.71	0.07	2.33		UOC-19661	0.9992	0.0014	-9.3	1.4	5	15
20	15	4.6	24.31	C-156308	1.14	0.07	1.91		UOC-19660	1.0092	0.0015	0.6	1.5	-70	15
2	15	5.2	23.48	C-156309	1.13	0.08	1.79		UOC-19659	1.0146	0.0015	5.9	1.5	-110	15
C014	***RadCARBBS***														
495	16	0.4	34.73	C-156624	0.36	0.05	2.48		UOC-19232	1.0470	0.0015	38.1	1.5	-365	15
396	16	0.3	34.70	C-156625	0.54	0.06	2.51	0.06	UOC-19230	1.0466	0.0015	37.7	1.5	-360	15
				C-156626	0.39	0.06	2.43		UOC-19231	1.0472	0.0015	38.2	1.5	-365	15
				C-156627	0.41	0.04	2.46								
297	16	0.2	34.59	C-156628	0.43	0.04	2.47		UOC-19229	1.0479	0.0015	39.0	1.5	-370	15

178	16	-0.9	33.45	C-156629	0.10	0.05	2.49		UOC-19228	1.0205	0.0015	11.8	1.5	-160	15
139	16	-1.2	32.82	C-156630	0.14	0.04	2.49		UOC-19226	1.0074	0.0014	-1.2	1.4	-55	15
99	16	-1.1	32.41	C-156631	0.30	0.05	2.43		UOC-19225	0.9979	0.0014	-10.6	1.4	15	15
42	16	-0.8	31.29	C-156632	1.27	0.04	2.33		UOC-19224	1.0018	0.0015	-6.8	1.5	-10	15
20	16	-0.2	30.73	C-156633	1.54	0.05	2.29		UOC-19223	1.0012	0.0014	-7.4	1.4	-5	15
3	16	4.4	28.67	C-156634	1.51	0.04	2.20		UOC-19222	1.0055	0.0014	-3.1	1.4	-40	15
405	***RadCARBBS***														
496	18	0.4	34.74	C-156295	0.34	0.04	2.44	0.01	UOC-20611	1.0437	0.0016	34.8	1.6	-340	15
				C-156296	0.35	0.01	2.42		UOC-20612	1.0442	0.0016	35.3	1.6	-345	15
				C-156297	0.36	0.03	2.46								
396	18	0.4	34.72	C-156298	0.33	0.03	2.42		UOC-20610	1.0438	0.0016	34.9	1.6	-340	15
298	18	0.3	34.66	C-156299	0.32	0.03	2.42		UOC-20609	1.0471	0.0016	38.2	1.6	-365	15
178	18	-0.5	34.00	C-156300	0.07	0.05	2.44		UOC-20608	1.0326	0.0016	23.8	1.6	-255	15
139	18	-1.0	33.41	C-156301	-0.02	0.03	2.46		UOC-20605	1.0177	0.0016	9.0	1.6	-135	15
99	18	-1.1	32.84	C-156303	0.04	0.03	2.46		UOC-20604	1.0047	0.0016	-3.8	1.6	-35	15
44	18	-0.7	31.91	C-156304	0.56	0.05	2.33		UOC-20603	0.9963	0.0016	-12.2	1.6	30	15
20	18	0.3	30.58	C-156302	1.43	0.04	2.24		UOC-20602	0.9995	0.0016	-9.0	1.6	5	15
4	18	2.9	27.85	C-156305	1.31	0.03	2.07		UOC-20601	0.9956	0.0016	-12.9	1.6	35	15
414	***RadCARBBS***														
294	27	0.3	34.65	C-156615	0.59	0.05	2.52		UOC-19676	1.0513	0.0015	42.3	1.5	-395	15
178	27	-0.9	33.45	C-156616	0.13	0.05	2.53		UOC-19675	1.0195	0.0014	10.8	1.4	-150	15
138	27	-1.2	32.91	C-156617	0.13	0.05	2.53		UOC-19674	1.0081	0.0014	-0.6	1.4	-60	15
99	27	-1.1	32.48	C-156618	0.38	0.06	2.53		UOC-19673	0.9957	0.0014	-12.8	1.4	35	15
49	27	-1.2	31.23	C-156619	1.37	0.06	2.37		UOC-19672	0.9957	0.0014	-12.8	1.4	35	15
19	27	0.1	28.56	C-156620	1.67	0.05	2.23		UOC-19670	0.9994	0.0014	-9.2	1.4	5	15
2	27	1.1	27.84	C-156622	1.54	0.06	2.14		UOC-19668	1.0021	0.0014	-6.5	1.4	-10	15
				C-156623	1.55	0.05	2.15	0.01							
				C-156621	1.55	0.06	2.16		UOC-19669	1.0021	0.0014	-6.4	1.4	-10	15
PCB07	***RadCARBBS***														
42	51	-1.0	31.71	C-156280	-0.29	0.05	2.51		UOC-19667	0.9953	0.0014	-13.2	1.4	40	15
12	51	2.4	29.83	C-156281	0.73	0.05	2.36		UOC-19666	0.9905	0.0014	-18.0	1.4	75	15

2	51	3.1	28.24	C-156282	0.86	0.04	2.26		UOC-19663	0.9885	0.0014	-20.0	1.4	95	15
434	***RadCARBBS***														
35	52	-1.0	31.69	C-156276	0.46	0.04	2.42		UOC-19861	0.9935	0.0015	-15.0	1.5	50	15
				C-156277	0.42	0.04	2.46	0.00							
				C-156275	0.43	0.06	2.46		UOC-19862	0.9945	0.0016	-14.0	1.6	45	15
15	52	-0.1	30.87	C-156278	1.51	0.05	2.30		UOC-19860	1.0020	0.0016	-6.6	1.6	-10	15
2	52	5.3	18.44	C-156279	-0.68	0.05	2.12		UOC-19859	0.9563	0.0016	-51.9	1.6	360	15
476	***RadCARBBS***														
178	82	-1.2	33.59	C-156267	0.08	0.08	2.54		UOC-20216	1.0194	0.0014	10.7	1.4	-150	15
139	82	-1.4	32.94	C-156269	0.12	0.05	2.50		UOC-20212	0.9936	0.0014	-14.9	1.4	50	15
				C-156270	0.14	0.05	2.49	0.02							
				C-156268	0.09	0.06	2.52		UOC-20213	0.9947	0.0014	-13.8	1.4	40	15
99	82	-1.3	32.48	C-156271	0.18	0.07	2.49		UOC-20211	0.9913	0.0014	-17.2	1.4	70	15
50	82	-0.8	31.48	C-156272	0.62	0.04	2.41		UOC-20210	0.9940	0.0014	-14.5	1.4	50	15
25	82	-0.5	30.47	C-156273	1.38	0.06	2.32		UOC-20209	0.9992	0.0014	-9.3	1.4	5	15
1	82	3.4	19.59	C-156274	-0.35	0.05	2.13		UOC-20206	0.9636	0.0014	-44.7	1.4	300	15
PCB12	***RadCARBBS***														
44	93	-0.9	31.48	C-156254	0.58	0.12	2.47		UOC-19867	0.9941	0.0016	-14.4	1.6	45	15
12	93	0.8	29.99	C-156255	1.46	0.08	2.21	0.03	UOC-19865	0.9983	0.0017	-10.3	1.7	15	15
				C-156256	1.45	0.09	2.25		UOC-19866	1.0006	0.0016	-7.9	1.6	0	15
				C-156257	1.48	0.08	2.21								
5	93	1.3	25.62	C-156258	1.06	0.08	2.13		UOC-19863	0.9934	0.0016	-15.1	1.6	55	15
546	***RadCARBBS***														
1598	97	-0.4	34.92	C-156239	1.05	0.07	2.42		UOC-19219	0.9478	0.0014	-60.3	1.4	430	15
1480	97	-0.3	34.89	C-156241	0.94	0.02	2.45		UOC-19217	0.9800	0.0014	-28.4	1.4	160	15
				C-156240	0.96	0.05			UOC-19218	0.9821	0.0014	-26.3	1.4	145	15
1184	97	-0.1	34.87	C-156243	0.96	0.06	2.47		UOC-19216	1.0076	0.0015	-1.1	1.5	-55	15
988	97	0.1	34.86	C-156244	0.89	0.06	2.45		UOC-19215	1.0248	0.0015	16.1	1.5	-190	15
790	97	0.3	34.85	C-156245	0.88	0.06	2.45		UOC-19212	1.0297	0.0015	20.9	1.5	-230	15
593	97	0.6	34.83	C-156246	0.77	0.03	2.47		UOC-19211	1.0459	0.0015	37.0	1.5	-355	15
396	97	0.5	34.74	C-156247	0.63	0.05	2.51		UOC-19210	1.0538	0.0015	44.8	1.5	-415	15

297	97	-0.2	34.39	C-156248	0.41	0.05	2.49		UOC-19209	1.0585	0.0015	49.5	1.5	-450	15
									UOC-20618	1.0535	0.0016	44.4	1.6	-415	15
198	97	-1.3	33.08	C-156249	0.20	0.05	2.53		UOC-19205	0.9863	0.0014	-22.1	1.4	110	15
99	97	-1.2	32.41	C-156250	0.14	0.05	2.46		UOC-19204	0.9933	0.0014	-15.2	1.4	55	15
50	97	-0.8	31.04	C-156251	1.17	0.05	2.34		UOC-19203	0.9996	0.0015	-8.9	1.5	5	15
30	97	-0.9	30.00	C-156252	1.43	0.03	2.31		UOC-19202	0.9995	0.0015	-9.1	1.5	5	15
3	97	-0.9	23.64	C-156253	0.83	0.05	2.02		UOC-19201	0.9926	0.0015	-15.9	1.5	60	15
515	***RadCARBBS***														
396	101	0.5	34.79	C-157003	0.66	0.06	2.55		UOC-20226	1.0405	0.0015	31.6	1.5	-315	15
297	101	0.2	34.65	C-157004	0.55	0.06	2.56		UOC-20225	1.0468	0.0014	37.9	1.4	-360	15
178	101	-0.8	33.91	C-157005	0.33	0.06	2.53		UOC-20224	1.0365	0.0014	27.6	1.4	-285	15
139	101	-1.3	33.11	C-157006	0.15	0.03	2.57		UOC-20223	1.0071	0.0014	-1.5	1.4	-50	15
99	101	-1.4	32.49	C-157008	0.24	0.04	2.53		UOC-20220	0.9911	0.0014	-17.3	1.4	70	15
				C-157009	0.16	0.02	2.54	0.02							
				C-157007	0.25	0.04	2.51		UOC-20222	0.9921	0.0014	-16.4	1.4	65	15
35	101	-1.1	31.08	C-157011	1.37	0.05	2.39		UOC-20219	1.0009	0.0014	-7.6	1.4	0	15
24	101	-1.2	30.38	C-157010	1.46	0.03	2.34		UOC-20218	1.0003	0.0014	-8.2	1.4	0	15
2	101	-1.4	28.43	C-157012	1.56	0.03	2.22		UOC-20217	1.0030	0.0014	-5.6	1.4	-20	15
518	***RadCARBBS***														
396	103	0.5	34.80	C-156993	0.58	0.04	2.53		UOC-20598	1.0315	0.0016	22.6	1.6	-245	15
300	103	0.4	34.76	C-156994	0.58	0.05	2.49		UOC-20597	1.0345	0.0016	25.7	1.6	-270	15
179	103	-0.8	33.83	C-156995	0.18	0.07	2.51		UOC-20596	1.0246	0.0016	15.8	1.6	-190	15
139	103	-1.3	33.23	C-156996	0.21	0.07	2.49		UOC-20595	1.0077	0.0016	-0.9	1.6	-55	15
99	103	-1.4	32.59	C-156997	0.18	0.05	2.51		UOC-20591	0.9890	0.0016	-19.5	1.6	90	15
50	103	-1.1	31.58	C-156998	1.01	0.06	2.36		UOC-20590	0.9902	0.0016	-18.3	1.6	80	15
30	103	-1.0	30.96	C-156999	1.58	0.04	2.35		UOC-20589	0.9945	0.0016	-14.0	1.6	45	15
2	103	-1.4	28.55	C-157000	1.60	0.04	2.26	0.00	UOC-20587	0.9998	0.0016	-8.8	1.6	0	15
				C-157001	1.60	0.03	2.26		UOC-20588	1.0014	0.0016	-7.2	1.6	-5	15
				C-157002	1.60	0.04	2.25								
193	***[1]Baffin Bay***														
787	5	1.0	34.50	C-143456	-0.12	0.03	2.21		UCIAMS-236301	1.0004	0.0012	-7.9	1.2	Modern	

592	5	1.5	34.50	C-143457	-0.10	0.05	2.21	UCIAMS-236302	1.0135	0.0013	5.1	1.3	Modern
				C-143458	-0.16	0.05							
393	5	3.0	34.55	C-143459	0.07	0.06	2.18	UCIAMS-236303	1.0270	0.0013	18.5	1.3	Modern
				C-143460	-0.05	0.08		UCIAMS-236304	1.0238	0.0013	15.3	1.3	Modern
196	5	4.4	34.61	C-143461	0.07	0.06	2.16	UCIAMS-236305	1.0257	0.0013	17.2	1.3	Modern
98	5	-0.9	33.57	C-143462	0.47	0.08	2.13	UCIAMS-236306	1.0291	0.0013	20.5	1.3	Modern
48	5	-1.3	33.16	C-143463	0.21	0.04	2.15	UCIAMS-236307	1.0246	0.0013	16.0	1.3	Modern
18	5	2.8	32.83	C-143464	1.47	0.05	2.02	UCIAMS-236308	1.0242	0.0014	15.7	1.4	Modern
3	5	-0.1	30.40	C-143465	1.06	0.05	1.98	UCIAMS-236312	1.0161	0.0016	7.6	1.6	Modern
196	***[1]Baffin Bay***												
97	9	1.4	33.75	C-143466	0.46	0.06	2.12	UCIAMS-236313	1.0290	0.0014	20.4	1.4	Modern
48	9	1.7	33.68	C-143467	0.43	0.05	2.11	UCIAMS-236314	1.0255	0.0016	17.0	1.6	Modern
18	9	2.6	33.59	C-143468	0.70	0.07	2.08	UCIAMS-236315	1.0314	0.0014	22.9	1.4	Modern
4	9	4.0	33.49	C-143469	1.01	0.06	2.05	UCIAMS-236316	1.0272	0.0014	18.7	1.4	Modern
				C-143470	1.05	0.06		UCIAMS-236317	1.0285	0.0013	20.0	1.3	Modern
BB15	***[1]Baffin Bay***												
394	12	3.7	34.57	C-143471	-0.13	0.03	2.17	UCIAMS-236318	1.0247	0.0015	16.2	1.5	Modern
197	12	3.0	34.36	C-143472	-0.09	0.07	2.16	UCIAMS-236319	1.0277	0.0014	19.2	1.4	Modern
98	12	0.9	33.92	C-143473	-0.22	0.06	2.16	UCIAMS-236320	1.0257	0.0014	17.2	1.4	Modern
48	12	-0.2	33.62	C-143474	0.35	0.04	2.09	UCIAMS-236321	1.0279	0.0017	19.4	1.7	Modern
18	12	5.4	33.54	C-143475	1.31	0.04	2.01	UCIAMS-236322	1.0270	0.0016	18.5	1.6	Modern
3	12	5.6	33.54	C-143476	1.32	0.04	2.02	UCIAMS-236323	1.0245	0.0020	15.9	2.0	Modern
BB18	***[1]Baffin Bay***												
396	14	1.9	34.26	C-143484	-0.30	0.02	2.18	UCIAMS-240010	1.0247	0.0017	16.2	1.7	Modern
196	14	1.3	34.03	C-143485	-0.22	0.03	2.17	UCIAMS-240011	1.0254	0.0016	16.9	1.6	Modern
98	14	0.7	33.72	C-143486	-0.18	0.03	2.14	UCIAMS-240012	1.0262	0.0017	17.6	1.7	Modern
48	14	0.9	33.32	C-143487	0.05	0.05	2.11	UCIAMS-240013	1.0301	0.0016	21.6	1.6	Modern
19	14	1.2	32.70	C-143488	0.38	0.07	2.04	UCIAMS-240014	1.0280	0.0016	19.4	1.6	Modern
				C-143489	0.21	0.02		UCIAMS-240019	1.0283	0.0018	19.7	1.8	Modern
3	14	4.4	31.06	C-143490	1.90	0.03	1.81	UCIAMS-240020	1.0266	0.0016	18.1	1.6	Modern
227	***[1]Baffin Bay***												

394	18	2.2	34.51	C-143491	-0.41	0.03	2.19	UCIAMS-237416	1.0230	0.0017	14.5	1.7	Modern	
				C-143492	-0.38	0.02		UCIAMS-237417	1.0229	0.0017	14.4	1.7	Modern	
197	18	1.8	34.22	C-143493	-0.28	0.02	2.17	UCIAMS-237418	1.0274	0.0015	18.8	1.5	Modern	
98	18	0.2	33.83	C-143494	-0.09	0.04	2.16	UCIAMS-237419	1.0263	0.0016	17.7	1.6	Modern	
48	18	-0.6	33.63	C-143495	0.44	0.06	2.14	UCIAMS-237420	1.0293	0.0016	20.8	1.6	Modern	
19	18	5.4	33.34	C-143496	1.41	0.03	2.06	UCIAMS-237421	1.0272	0.0014	18.6	1.4	Modern	
4	18	5.4	33.34	C-143497	1.40	0.04	2.02	UCIAMS-237422	1.0288	0.0016	20.2	1.6	Modern	
224	***[1]Baffin Bay***													
1969	24	-0.3	34.50	C-143513	-0.68	0.04	2.28	UCIAMS-237436	0.9181	0.0013	-89.5	1.3	685	15
1773	24	-0.3	34.49	C-143514	-0.43	0.04	2.27	UCIAMS-237437	0.9210	0.0013	-86.7	1.3	660	15
1576	24	-0.1	34.49	C-143515	-0.43	0.02	2.26	UCIAMS-237438	0.9257	0.0013	-82.0	1.3	620	15
1380	24	0.2	34.49	C-143516	-0.52	0.04	2.25	UCIAMS-237439	0.9344	0.0015	-73.4	1.5	545	15
1183	24	0.5	34.49	C-143517	-0.43	0.06	2.23	UCIAMS-237440	0.9554	0.0014	-52.6	1.4	365	15
986	24	0.8	34.49	C-143518	-0.27	0.05	2.22	UCIAMS-237441	0.9857	0.0015	-22.5	1.5	110	15
				C-143519	-0.25	0.03		UCIAMS-237442	0.9862	0.0015	-22.0	1.5	115	15
				C-143520	-0.30	0.02								
789	23	1.3	34.52	C-143498	-0.10	0.04	2.21	UCIAMS-237423	1.0013	0.0015	-7.0	1.5	Modern	
				C-143499	-0.12	0.05		UCIAMS-237425	1.0046	0.0015	-3.7	1.5	Modern	
592	23	1.7	34.52	C-143500	-0.11	0.04	2.20	UCIAMS-237426	1.0159	0.0014	7.5	1.4	Modern	
394	23	1.9	34.43	C-143501	-0.14	0.05	2.19	UCIAMS-237427	1.0282	0.0015	19.6	1.5	Modern	
197	23	-0.6	33.78	C-143502	-0.08	0.04	2.17	UCIAMS-237428	1.0266	0.0014	18.1	1.4	Modern	
98	23	-1.7	33.13	C-143503	0.26	0.03	2.16	UCIAMS-237429	1.0238	0.0013	15.3	1.3	Modern	
48	23	-1.7	32.90	C-143504	0.39	0.04	2.15	UCIAMS-237430	1.0165	0.0015	8.1	1.5	Modern	
19	23	-1.4	32.41	C-143511	0.34	0.06	2.13	UCIAMS-240021	1.0162	0.0018	7.7	1.8	Modern	
3	23	0.0	29.68	C-143512	0.69	0.07	1.96	UCIAMS-237432	1.0172	0.0015	8.7	1.5	Modern	
BB2	***[1]Baffin Bay***													
2262	30	-0.3	34.50	C-144095	-0.29	0.05	2.28	UCIAMS-236333	0.9169	0.0013	-90.7	1.3	685	15
				C-144096	-0.30	0.05		UCIAMS-236334	0.9184	0.0012	-89.2	1.2	695	15
1968	30	-0.3	34.49	C-144097	-0.27	0.04	2.27	UCIAMS-236335	0.9186	0.0013	-89.1	1.3	680	15
1772	30	-0.2	34.49	C-144098	-0.36	0.04	2.26	UCIAMS-236338	0.9234	0.0011	-84.3	1.1	640	15
1576	30	0.0	34.49	C-144099	-0.30	0.03	2.26	UCIAMS-236339	0.9279	0.0012	-79.9	1.2	600	15

1380	30	0.4	34.49	C-144100	-0.25	0.04	2.24	UCIAMS-236340	0.9432	0.0013	-64.6	1.3	470	15
1183	30	0.7	34.49	C-144101	-0.16	0.02	2.21	UCIAMS-236341	0.9726	0.0012	-35.4	1.2	225	15
986	30	1.2	34.51	C-144102	-0.17	0.04	2.21	UCIAMS-236342	0.9892	0.0013	-19.0	1.3	85	15
789	29	1.7	34.53	C-143521	-0.09	0.03	2.21	UCIAMS-236324	1.0142	0.0014	5.7	1.4	Modern	
592	29	1.4	34.43	C-143522	-0.03	0.05	2.21	UCIAMS-236325	1.0291	0.0014	20.6	1.4	Modern	
394	29	1.4	34.36	C-143523	-0.13	0.03	2.20	UCIAMS-236326	1.0281	0.0013	19.6	1.3	Modern	
197	29	0.2	34.00	C-143524	-0.01	0.04	2.16	UCIAMS-236327	1.0295	0.0014	21.0	1.4	Modern	
98	29	-1.4	33.42	C-143525	0.26	0.03	2.15	UCIAMS-236328	1.0295	0.0013	20.9	1.3	Modern	
48	29	-1.7	33.04	C-143526	0.24	0.04	2.16	UCIAMS-236329	1.0184	0.0015	10.0	1.5	Modern	
19	29	-0.9	31.94	C-143527	0.92	0.04	2.10	UCIAMS-236330	1.0142	0.0013	5.8	1.3	Modern	
3	29	2.2	29.81	C-143528	1.16	0.02	1.94	UCIAMS-236331	1.0153	0.0015	6.8	1.5	Modern	
				C-143529	1.15	0.04		UCIAMS-236332	1.0130	0.0014	4.6	1.4	Modern	
				C-143530	1.12	0.03								
204	***[1]Baffin Bay***													
789	34	1.3	34.50	C-144115	-0.15	0.02	2.20	UCIAMS-237455	1.0058	0.0015	-2.5	1.5	Modern	
				C-144116	-0.15	0.04		UCIAMS-237456	1.0032	0.0016	-5.1	1.6	Modern	
592	34	1.5	34.49	C-144117	-0.04	0.03	2.20	UCIAMS-237457	1.0161	0.0017	7.7	1.7	Modern	
396	34	1.6	34.40	C-144118	-0.02	0.06	2.19	UCIAMS-237458	1.0180	0.0015	9.6	1.5	Modern	
				C-144119	0.00	0.04								
196	34	0.7	34.03	C-144120	-0.09	0.03	2.18	UCIAMS-237459	1.0268	0.0015	18.2	1.5	Modern	
98	34	-0.5	33.69	C-144121	0.14	0.04	2.18	UCIAMS-237460	1.0301	0.0015	21.6	1.5	Modern	
45	34	-0.8	33.39	C-144122	0.37	0.05	2.14	UCIAMS-237461	1.0255	0.0015	17.0	1.5	Modern	
18	34	2.8	32.81	C-144123	1.73	0.04	2.00	UCIAMS-237462	1.0238	0.0014	15.3	1.4	Modern	
4	34	7.3	32.17	C-144124	1.35	0.03	2.00	UCIAMS-237463	1.0230	0.0014	14.5	1.4	Modern	
								UCIAMS-237464	1.0227	0.0015	14.2	1.5	Modern	
210	***[1]Baffin Bay***													
1063	37	1.3	34.51	C-144125	-0.21	0.02	2.21	UCIAMS-237446	1.0021	0.0015	-6.2	1.5	Modern	
				C-144126	-0.17	0.03		UCIAMS-237447	1.0036	0.0014	-4.8	1.4	Modern	
789	37	1.5	34.52	C-144127	-0.12	0.03	2.21	UCIAMS-237448	1.0028	0.0015	-5.5	1.5	Modern	
591	37	1.7	34.52	C-144128	-0.10	0.03	2.21	UCIAMS-237449	1.0073	0.0015	-1.1	1.5	Modern	
394	37	1.9	34.42	C-144129	-0.16	0.04	2.20	UCIAMS-237450	1.0178	0.0015	9.3	1.5	Modern	

197	37	0.4	33.98	C-144130	-0.02	0.04	2.18	UCIAMS-237451	1.0285	0.0016	20.0	1.6	Modern
				C-144131	-0.10	0.05							
98	37	-0.5	33.68	C-144132	0.11	0.04	2.16	UCIAMS-237454	1.0238	0.0016	15.3	1.6	Modern
48	37	-0.9	33.45	C-144133	0.20	0.04	2.14	UCIAMS-237443	1.0260	0.0015	17.5	1.5	Modern
18	37	0.0	33.13	C-144134	1.11	0.02	2.06	UCIAMS-237444	1.0253	0.0015	16.8	1.5	Modern
3	37	9.5	32.94	C-144135	1.52	0.04	2.03	UCIAMS-237445	1.0244	0.0015	15.9	1.5	Modern
108	***[1]Baffin Bay***												
394	53	-0.1	34.34	C-144150	0.15	0.03	2.18	UCIAMS-236343	1.0388	0.0014	29.4	1.4	Modern
				C-144151	-0.02	0.03		UCIAMS-236344	1.0380	0.0014	30.1	1.4	Modern
295	53	-0.1	34.25	C-144152	-0.10	0.01	2.18	UCIAMS-236345	1.0368	0.0013	28.2	1.3	Modern
196	53	-0.4	33.94	C-144153	-0.11	0.05	2.16	UCIAMS-236346	1.0329	0.0013	24.3	1.3	Modern
97	53	-1.3	32.92	C-144154	0.24	0.05	2.14	UCIAMS-236347	1.0121	0.0013	3.7	1.3	Modern
48	53	-1.5	32.36	C-144155	0.22	0.03	2.13	UCIAMS-236348	1.0147	0.0014	6.3	1.4	Modern
18	53	1.8	31.58	C-144156	1.14	0.04	2.02	UCIAMS-236349	1.0078	0.0013	-0.6	1.3	Modern
				C-144157	1.19	0.03							
2	53	3.1	31.14	C-144158	1.42	0.02	1.98	UCIAMS-236350	1.0029	0.0016	-5.4	1.6	Modern
323	***[1]Baffin Bay***												
740	66	0.6	34.46	C-144163	0.00	0.04	2.14	UCIAMS-240002	1.0161	0.0016	7.7	1.6	Modern
592	66	0.9	34.46	C-144159	-0.09	0.03	2.20	UCIAMS-239998	1.0181	0.0016	9.6	1.6	Modern
394	66	0.9	34.35	C-144160	-0.08	0.07	2.19	UCIAMS-239999	1.0315	0.0016	22.9	1.6	Modern
196	66	-1.1	33.75	C-144161	0.07	0.03	2.18	UCIAMS-240000	1.0260	0.0016	17.5	1.6	Modern
98	66	-1.3	32.91	C-144162	0.18	0.04	2.16	UCIAMS-240001	1.0203	0.0015	11.8	1.5	Modern
48	66	-1.7	32.57	C-144164	0.39	0.03	2.17	UCIAMS-240003	1.0067	0.0017	-1.7	1.7	Modern
				C-144165	0.35	0.04							
19	66	-1.0	32.16	C-144166	0.71	0.04	2.04	UCIAMS-240007	1.0109	0.0016	2.5	1.7	Modern
				C-144167	0.71	0.03		UCIAMS-240008	1.0077	0.0017	-0.6	1.6	Modern
2	66	2.0	30.16	C-144168	1.49	0.05	1.92	UCIAMS-240009	1.0070	0.0016	-1.5	1.6	Modern

[1]Zeidan et al., 2022

Table S3. Core hydrographic and dissolved inorganic carbon (DIC) values of specific water masses observed in the Canadian Arctic Archipelago (CAA) and Baffin Bay. Depth, potential density (σ_θ), temperature and salinity values/ranges are adapted from literature to more simply group values observed during sample collection. Due to the high variability of water mass modification in the CAA and Baffin Bay, as well as variable published core hydrographic values, we prioritize σ_θ ranges when organizing DIC concentrations, $\delta^{13}C$ and $\Delta^{14}C$ results into specific water masses.

Water Mass	Depth (m)	σ_θ (kg m^{-3})	Temp (°C)	Salinity	[DIC]	$\delta^{13}C$ (‰)	$\Delta^{14}C$ (‰)
SML	[1] 0-40	< 24.5	-2 to 6	< 31	1.79 to 2.39	-0.68 to 1.86	-51.9 to 19.7
PSW	[1] 40-80	[5] 24.5 to 26	-0.8 to -1.2	[1]31 to 32	2.24 to 2.56	-0.29 to 1.58	-18.3 to 5.8
PWW	[1] 80-200	[4] 26 to 27	[4] -1 to -1.4	[4] 32 to 34	2.38 to 2.62	-0.02 to 0.45	-22.1 to 15.9
ATL_{FS}	[1] 200-1500	[4] 27 to 28	[4] 0 to 0.8	[4] 34 to 34.8	2.42 to 2.65	0.07 to 0.89	10.7 to 49.5
BIC	40-300	26 to 27.5	[3] < -1.6	[3] 32.5 to 33.8	2.09 to 2.18	-0.28 to 0.47	-1.7 to 24.3
WGIW	[2] 300-1200	[2] 27.3 to 27.7	[2] > 2	[2]34.1 to 34.5	2.14 to 2.23	-0.43 to 0.07	-52.6 to 29.8
CBDW	[1] > 1500	> 28	< 0	> 34.8	2.42 to 2.47	0.95 to 1.05	-60.3 to -1.1
BBDW	[2] > 1200	[2] > 27.7	[2] < 0	[2] > 34.5	2.24 to 2.28	-0.68 to -0.25	-90.0 to -64.6

[1]McLaughlin et al., 2005

[2] Curry et al., 2011

[3] Münchow et al., 2015

[4] Lehmann et al., 2022

[5] Watanabe, 2011

Table S4. Single factor one-way analysis of variance (ANOVA) test results for sections 4.2.3 (DIC isotopic shifts within Parry Channel from M'Clure Strait to Lancaster Sound) and 4.3 (Constraining the "Suess Effect" and Rates of Anthropogenic Carbon Penetration in the Arctic Ocean Between 2009-2021).

Section	Variable	ANOVA Test	Confidence Interval (%)	*df* (Between Groups, Within Groups)	*F*	*p value*
4.2.3	σ_θ	SML West/East	90	(1,3)	0.85	0.42
		PSW West/East		(1,3)	1.99	0.25
		PWW West/East		(1,4)	0.09	0.78
	[DIC]	SML West/East	90	(1,3)	1.29	0.34
		PSW West/East		(1,3)	20.81	0.02
		PWW West/East		(1,4)	2.90	0.16
	$\delta^{13}C$	SML West/East	90	(1,3)	8.94	0.06
		PSW West/East		(1,3)	7.27	0.07
		PWW West/East		(1,4)	54.87	0.00
	$\Delta^{14}C$	SML West/East	90	(1,3)	33.64	0.01
		PSW West/East		(1,3)	11.15	0.04
		PWW West/East		(1,4)	6.51	0.06
4.3	σ_θ	SML/PSW	95	(1,11)	8.21	0.02
		PSW/PWW		(1,12)	45.50	2.06E-05
		PWW/ATL_{FS}		(1,15)	173.97	1.18E-09
		ATL_{FS}/CBDW		(1,13)	13.10	3.12E-03
	$\Delta^{14}C$	SML 2009/2012/2021	95	(2,3)	22.25	0.02
		PSW 2009/2012/2021		(2,3)	84.44	2.31E-03
		PWW 2009/2012/2021		(2,5)	3.18	0.13
		PWW 2009/2021		(1,4)	5.03	0.09
		ATL_{FS} 2009/2012/2021		(2,6)	5.00	0.05
		CBDW 2009/2012/2021		(2,3)	0.22	0.81